

DYNAMICAL DIFFRACTION THEORY
WITH
X-RAY RESONANCE SCATTERING
AND ITS
APPLICATION

X線共振散乱を用いた物理学の発展とその応用

SHIMENZU TADASHI
1914-1983

①

DYNAMICAL-DIFFRACTION THEORY

WITH

X-RAY RESONANCE SCATTERING

AND ITS

APPLICATION

X線共鳴散乱を伴う動力学回折理論とその応用

RIICHIROU NEGISHI

根岸利一郎

Acknowledgements

During the course of this study, I owe many people for various aspects of the work. Among them, I would like to thank Prof. Tomoe Fukamachi of Saitama Institute of Technology (SIT) for his encouragement and useful suggestions. I would like to express my thanks to my collaborators, Prof. Masayasu Tokonami of SIT, and Prof. Takaaki Kawamura of Yamanashi University for their useful advice, and collaboration on this work, Prof. Tetsuo Nakajima of KEK-PF for his useful advice and help of the experiment in KEK-PF.

I also would like to thank Dr. Toshio Sakamaki of JEOL Ltd., Dr. Masami Yoshizawa of SIT, Mr. Isao Matsumoto of Graduate University for Advanced Studies, Prof. Zongyan Zhao and Prof. Shengming Zhou of Anhui University, Mr. Zhangcheng Xu of Shanghai Institute of Ceramics and Mr. Zeming Qi of Anhui University for useful discussions. I would like to thank Prof. Kenji Ehara of SIT for help in the sample processing.

I am grateful to Saburou Yaginuma of the library in SIT for his help for collecting the references. I am grateful to under graduates of Fukamachi Laboratory in SIT for their help to construct the experimental equipment and their assistance in experiments. I am grateful to Mr. Nobutaka Kamei of the machine shop of SIT for making the small rotating goniometer. I would like to thank Ms. Kiyomi Matsumoto of the secretary in Fukamachi Laboratory for her help in preparing this thesis.

Abstract

The conventional dynamical theory is developed under assumption that the resonance (anomalous) scattering is sufficiently small compared with the normal (Thomson) scattering. It has been very useful to the study of precise X-ray optics. By using X-ray from synchrotron radiation, it is now possible to study dynamical diffraction very near the absorption edge of a constituent atom in a crystal. The contribution of resonance scattering can be changed by tuning the X-ray energy. In an extreme case, the dynamical diffraction can be observed only due to the resonance scattering.

In the conventional dynamical theory, however, a parameter in the theory diverges when only the resonance scattering term exists without the normal scattering. Fukamachi and Kawamura [*Acta Cryst.*(1993). A49,384-388] have modified a dynamical theory to avoid the divergence, and derived the formula which is valid in calculating the diffraction intensity in general including the diffraction only due to the resonance scattering. In this paper, we have carried out the following study on the basis of idea of Fukamachi and Kawamura.

(1) At first, the principle of the conventional dynamical theory and the outline of its development are described. Secondly, the limitation of the theory in relation to the Borrmann effect or resonance scattering is pointed out. Thirdly, X-ray resonance scattering and the anomalous-scattering factors are discussed.

(2) The fundamental equations are derived following the method of Ewald-Laue. Then, the equations for examining the diffracted intensity, a dispersion surface, a Poynting vector and the wave field in a crystal are also derived. These equations are examined in detail in Laue case as well as in Bragg case. It is suggested that the dynamical diffraction by the resonance scattering without the ordinary scattering process.

(3) The simulated results by using the theory described in above (2) are verified by experiments. Four experiments are carried out. The first is to determine the phase change in rocking curves, the second is to measure the fluorescence X-rays, the third is the improvement of topographies, and the last one is the determination of anomalous scattering factors. Then, the conclusions are drawn, and some future views are described.

The present theory is not only applied to the Thomson scattering and the resonance scattering of X-ray, but also to the neutron and nuclear Bragg scattering due to the resonance scattering.

Contents

CHAPTER I INTRODUCTION

1.1 Introductory	1
1.1.1 Introductory	1
1.1.2 Outline of this paper	2
1.2 Outline of Conventional Dynamical Theory	4
1.2.1 Theories of Darwin and Ewald-Laue	5
1.2.2 Dynamical Theory with Small Resonance Scattering	6
1.2.3 Dispersion Surface in Two-Wave Approximation	8
1.2.4 Wave Field in Crystal	10
(i) Pendellösung beat	10
(ii) Borrmann effect and standing waves in a crystal	11
1.3 X-ray Resonance Scattering and Anomalous-Scattering Factor	12
1.4 Purpose of Study	21
1.4.1 Observation of Pendellösung Beat with X-ray Resonance Scattering and Breakdown of SIA	21
(i) Previous works	21
(ii) Present work	23
1.4.2 Circumstances of Study	24

CHAPTER II DYNAMICAL THEORY WITH RESONANCE SCATTERING

2.1 Fundamental Equations	29
2.1.1 X-Ray Electric Susceptibility without Absorption	29
2.1.2 X-Ray Electric Susceptibility with Absorption	32
2.1.3 Fundamental Equations	33

2.2 Solution of Fundamental-Equations	34
2.2.1 One-Wave Approximation	34
2.2.2 Two-Wave Approximation	35
(i) Solutions of two-wave approximation	37
(ii) When there is no absorption	38
(iii) When absorption cannot be neglected	40
(iv) Equation of the dispersion surface	41
(v) Comparison with present theory and SIA about form of dispersion surface	42
(vi) Diagrammatic presentation of two-wave approximation	44
2.2.3 Boundary Conditions	45
2.2.4 Diffraction Intensity	48
(i) Introductory	48
(ii) Diffracted intensity and transmitted intensity	52
(iii) Integrated reflecting power	54
2.2.5 Energy Flow	55
2.2.6 Wave Field in Crystal	55
(i) Pendellösung beat	55
(ii) Standing wave in a crystal	56
2.3 Diffracted Wave and Transmitted Wave in Laue Case	57
2.3.1 Rocking Curve	57
(i) Dependence on q	57
a) In case of $q=0$	57
b) In case of $q=1$	60
c) In case of $q=0.5$	62
(ii) Dependence on crystal thickness H	63
a) In case of $q=0$ ($g=-0.1$)	63

b) <i>In case of $q=0.5$ ($g_0=-1$)</i>	65
c) <i>In case of $q=1$ ($g_0=-1$)</i>	66
(iii) Dependence on $g(g_0)$	68
(iv) Dependence on phase difference δ	69
(v) Integrated reflecting power	71
2.3.2 Nontransparent Effect	72
2.3.3 Dispersion Surface in Laue Case	79
(i) Introductory	79
(ii) In case of $q=1$	80
a) <i>When normal-line v is located in $X \geq X(W =1)$</i>	81
b) <i>When normal-line v is located in $X <X(W =1)$</i>	84
(iii) In case of $q=0$	86
(iv) In case of $q=0.5$	87
2.3.4 Energy Flow	89
(i) The direction of the energy flow	89
a) <i>In case of $q=0$</i>	93
b) <i>In case of $0.5<q<1$</i>	93
c) <i>In case of $q=1$</i>	93
(ii) Quantitative treatment of the energy flow	94
a) <i>In case of $q=0$</i>	96
b) <i>In case of $q=0.5$</i>	96
c) <i>In case of $q=0.99$</i>	97
2.3.5 Wave Field in Crystal	98
(i) Phase of the pendellösung beat in $q=0$ and $q=1$	98
(ii) A pendellösung beat and crystal structure factor	99
(iii) A pendellösung beat and anomalous transmission (disappearance of the beat)	102

(iv) Standing wave	106
a) In case of $q=0$	107
b) In case of $q=1$	111
2.4. Diffracted Wave and Transmitted Wave in Bragg Case	117
2.4.1 Rocking Curve	117
(i) Dependence on q	117
a) In case of $q=0$	117
b) In case of $q=0.1$ and $q=0.5$	119
c) In case of $q=1$	120
(ii) Dependence on the crystal thickness	121
a) In case of $q=0$	121
b) In case of $q=0.5$	121
c) In case of $q=1$	122
d) Semi-infinite crystal	125
(iii) Dependence on $g(g_0)$	126
(iv) Dependence on phase difference δ	127
2.4.2 Dispersion Surface in Bragg Case	129
(i) In case of $q=0$	129
(ii) In case of $q=1$	131
(iii) In case of $q=0.01$ and $q=0.5$	132
2.4.3 Energy flow	132
2.4.4 Wave Field in Crystal	136
(i) In case of $q=0$	136
(ii) In case of $q=1$	138

CHAPTER III EXPERIMENTAL

3.1 Dynamical Diffraction due to $\chi_{hr}=0$ in Simple Substance	147
3.2 χ_{hr} and χ_{hi} for GaAs 200 near Ga and As K -Absorption Edges	149
3.3 Experimental System and Specimen	151
3.3.1 Experimental System	151
3.3.2 Specimen	152
3.4 Measurement of Rocking curves	152
3.4.1 Observation of δ and Dynamical Diffraction for $q \geq 0.5$	152
(i) Measured Rocking Curves for GaAs 200	152
(ii) Yield curves of fluorescence X-rays as a function of W	154
a) Experiment	154
b) Theory	156
c) Discussion	159
<In case of $q=1$ >	159
<In case of $q=0.5$ >	160
3.4.2 Observation of δ and Dynamical Diffraction for $q < 0.5$	161
(i) Measured rocking curves of transmitted wave for GaAs 200	161
(ii) The measured and simulated rocking curves for GaAs 600	164
3.5 Improvement of Contrast in Topography	169
3.5.1 Introductory	169
3.5.2 Experiment	169
3.6 Determination of Anomalous-Scattering Factors by Measured Rocking-Curves of Transmitted Wave near Absorption Edge	172
3.6.1 Observation of Rocking Curves for GaAs 200	172
3.6.2 Experiment	173
3.6.3 Fitting Analysis	176

3.6.4 Results and discussion	177
3.7 Summary	179

CHAPTER IV CONCLUSION AND FUTURE VIEW

4.1 Conclusions	185
4.2 Future View	186

CHAPTER I INTRODUCTION

1.1 Introductory

1.1.1 Introductory

Due to the need for the micronization of semiconductor devices and smaller sized devices such as nanoscale devices, the crystal perfection of semiconductors has been improved in recent years. For evaluating the crystal perfection, the intensity of X-ray diffraction from the semiconductor surfaces is widely used as a quite reliable technique. For analyzing the X-ray diffraction intensity from a perfect crystal or a nearly perfect crystal, the so-called dynamical theory of X-ray diffraction should be applied. In X-ray dynamical diffraction, one of the most characteristic effect is Borrmann effect (1941,1950) [1], which is peculiar to the dynamical diffraction with absorption taken into account. The Borrmann effects is conspicuous when the energy of X-rays is tuned near the absorption edge of a constituent atom in a crystal. In order to investigate the Borrmann effect by varying the energy near the absorption edge, or for the absorption edges of some atoms in a crystal, the X-ray source having continuous spectrum is required.

X-rays from synchrotron radiation (SR) is quite ideal for this purpose. The spectrum of the light from SR constitutes smooth continuum extending from ultra violet to X-ray. The brilliance is higher than the conventional source from X-ray tube by about 10,000 times or more. By using X-rays from SR, it is now possible to study Borrmann effect, or more generally speaking the effect of resonance scattering experimentally. However, in treating the resonance scattering, most conventional dynamical theories cannot be applied straightforwardly, because weak absorption is assumed in those theories.

In this paper, the limitation of the conventional dynamical theory is elucidated at first, and an alternative theory is introduced by modifying the conventional one to overcome the

limitation.

1.1.2 Outline of this paper

Chapter I "INTRODUCTION": At first, the principle of the conventional dynamical theory and the outline of its development are described. Secondly, the limitation of the theory in relation to the Borrmann effect or resonance scattering is pointed out. Thirdly, X-ray resonance scattering and anomalous-scattering factor are discussed. Then the purpose of present study is presented.

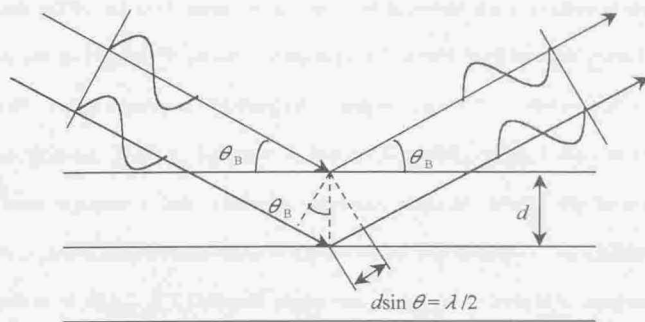
Chapter II "DYNAMICAL THEORY WITH THE RESONANCE SCATTERING": In this chapter, fundamental equations are derived following the method of Ewald-Laue. Then, and the equations for the diffracted intensity, the dispersion surface, the Poynting vector and the wave field in a crystal are derived. And these equations are used to examine dynamical diffractions involving resonance scattering in detail about both in Laue case and Bragg case. It is found that the dynamical diffraction only due to X-ray resonance scattering without the ordinary scattering process occurs at a certain energy near an absorption edge.

Chapter III "EXPERIMENTAL": In this chapter, the simulated results by using the theory described in chapter II are verified by experiments. Four Experiments are carried out. The first is to determine the phase change in rocking curves, the second is to measure the fluorescence X-rays, the third is the improvement of topographys, and the last one is the determination of anomalous scattering factors. Then the conclusions are drawn, and some future views are described.

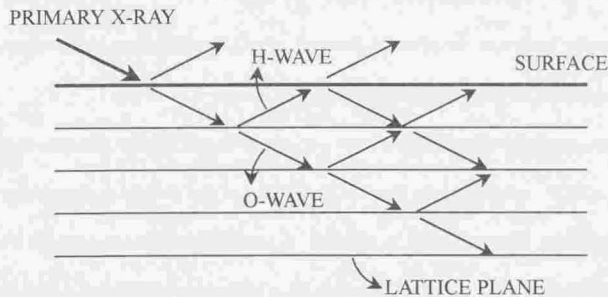
Chapter I and Chapter II are intended to review the conventional dynamical theory and to introduce a modified theory applicable to more general cases including not only strong absorption but also no real part of Fourier coefficient of X-ray polarizability. Assumptions

and approximations were examined in detail for the basic equations of the theory which were directly derived from Maxwell's equation in vacuum. The theory of the second half of the Chapter II after 2.2.4 is the original description by the present author. This theory is applied to Laue Case and Bragg Case, and is examined in detail. Rocking curves as a function of the crystal thickness has been examined, and a nontransparent effect is presented(2.3.2). A complex dispersion surface is introduced to elucidate such phenomena as absorption, the pendellösung beat and phase change(2.3.3, 2.4.2). In examination of Poynting vector, the conventional concept that the direction of the energy flow is always normal to the dispersion surface breaks down(2.3.4, 2.4.3). The disappearance of the pendellösung beat, and the phase difference of $\pi/2$ in a standing wave are found out at a certain condition of the constituent atom(2.3.5, 2.4.4).

Several simulations and experiments performed by the author are described in Chapter III. In GaAs200 reflection, the Fourier coefficient of the electric susceptibility near Ga K-absorption edge is numerically calculated. It was found in the simulation that the phase difference δ changes from 0, π , 0 to $-\pi$ (3.2) as a function of X-ray energy across Ga and As K-absorption edges. The simulated result is verified by the following four experiments: ①the observed rocking curves in Laue case, ②the intensity changes of the fluorescence X-rays depending on the incident X-ray energy(3.3.3), ③the observed rocking curves below Ga K-absorption edge for GaAs200 in Laue case as well as for ④ GaAs600 in Bragg case(3.3.4). In topographic observation when the resonance scattering is strong in GaAs 200, the contrast has been remarkably improved compared with that of weak absorption(3.3.5). Rocking curves in Laue case are observed, and anomalous-scattering factors were determined by using a profile fitting method(3.3.6).



(a) Single scattering



(b) Multiple scattering

Fig 1.1 The X-ray scattering by the crystal

1.2 Outline of Conventional Dynamical Theory

The diffraction of the X-rays by crystal was first discovered by the experiment of Friedrich, Knipping and Laue[2]. The process of the X-ray scattering is understood as follows: firstly, when X-rays are incident into a crystal, the electron in a material vibrates and the electromagnetic field is excited, secondly, the current produced by the vibration emits an electromagnetic field[3]. An X-ray diffraction phenomenon is explained by two

alternative theories: kinematical and dynamical theory. The diffraction by a fine crystal which has the size (several micrometers) less than an X-ray extinction distance (refer to [2]) is interpreted by the kinematical theory, or the single scattering theory(Fig.1.1 (a)). The theory is widely used for the crystal structural analysis. On the other hand, the diffraction of a perfect crystal which does not have defect the size of X-ray extinction distance should be described by a multiple scattering theory(Fig.1.1 (b)). The diffraction with such a multiple scattering is interpreted by the dynamical theory. Here, we investigate the development of the conventional dynamical theory, and the approximation, and then briefly describe the dispersion surface and the wave field.

1.2.1 Theories of Darwin and Ewald-Laue

The study of dynamical theory was started first by Darwin (1914)[4]. Darwin gave the constant difference equation (Darwin's equation) from which the amplitude of the reflection from each lattice plane parallel to crystal surfaces, and the amplitude of forward scattering are obtained. He derived the reflection curve (rocking curve) and the integrated reflecting power from a perfect crystal of the thickness of semi-infinity. The *scatter*(σ) of a *reflexion curve* angle was as small as about 10 seconds, and a integrated reflecting powers was much smaller than the measured result. Therefore the real crystal was interpreted as an imperfect crystal[5].

On the other hand, Ewald(1917)[6] treated the interaction of dipole waves and electromagnetic waves. The underlying idea of his theory is stated briefly as follows. Each lattice-point of the crystal is supposed to be occupied by a dipole which can be set into oscillation by the radiation field of any electromagnetic wave passing through the crystal. The oscillating dipoles themselves emit radiation, which produces a radiation field. The

self-consistent electric field in which this relationship is satisfied with all the dipoles in a crystal should be realized. Laue(1931)[7] made the theory of Ewald more simply. Ewald's theory was taken as a set of discontinuous dipoles within a crystal. However, Laue replaced it by the continuous and periodic polarization. And he solved the Maxwell's equation. The methods used by Ewald and Laue were different, but the results of them are essentially the same. These methods can be handled simpler than Darwin's theory. For this reason, their methods are used widely today in general studies. The method of Ewald-Laue is used in this paper.

1.2.2 Dynamical Theory with Small Resonance Scattering.

There are two competitive mechanisms in elastic scattering of X-rays: Thomson scattering (depends on electron density distribution, and is called *normal scattering* in this paper) and resonance scattering. The atomic scattering factor in the normal scattering is called normal scattering factor and is expressed by f^0 in this paper (usually expressed by f_0). f^0 can be calculated by the following equation

$$f^0(s) = \int \rho(r) \exp(is \cdot r) dr \quad (1.1)$$

Where, $\rho(r)$ is electron density and r is the distance from the nucleus. $f^0(s)$ decreases monotonously as " s " increases. Assuming that atoms are spherically symmetric, the magnitude of " s " is written as $|s| = 4\pi \sin \theta / \lambda$. Here, θ is a half of the scattering angle, and λ is the wavelength of X-ray. If θ is zero, $f^0(0)$ is equal to the atomic number Z , and is the maximum.

Conventionally, the resonance scattering is the scattering with the anomalous dispersion. It has customarily been called *anomalous scattering*. Scattering factor due to resonance

scattering is called *anomalous-scattering factor*. The anomalous-scattering factor is a function of the X-ray energy(ω) and can be expressed by the following equation

$$f'(\omega) + if''(\omega) \quad (1.2)$$

When ω approaches the absorption edge ω_K of a scattering atom, these quantities f' and f'' become the same order as $f^0(s)$. However, in the case of $\omega_K \ll \omega$, these quantities are quite small, and they are negligible. The X-ray resonance scattering is related to the photoelectric absorption which is main absorption of X-rays, closely. Therefore, if the photoelectric absorption is large, the magnitude of anomalous-scattering factor becomes large. If the X-ray resonance scattering is small, the photoelectric absorption also becomes small.

When atomic scattering factor $f(s, \omega)$ contains the normal scattering and the X-ray resonance scattering, it is written by the following equation

$$f(s, \omega) = f^0(s) + f'(\omega) + if''(\omega) \quad (1.3)$$

In the diffraction experiment by the characteristic X-rays from the conventional X-ray tube, the energy of the incident X-rays cannot always be tuned near the absorption edge of a constituent atom in a crystal. For this reason, the diffraction by the normal scattering has been main element and X-ray resonance scattering has been handled afterward as correction to it. In the conventional dynamical theory, the normal scattering is first treated and X-ray resonance scattering is treated as a correction. The atomic scattering factor is considered as in the following approximation

$$|f^0 + f'| > |f''| \quad (1.4)$$

This approximation is called *small imaginary part approximation*(SIA)[8]. SIA means that the real part of atomic scattering factors is larger than that of the imaginary part, and that the cases of $f'' = 0$ and $f' = 0$ are induced as the extreme. Almost all the dynamical

effects are derived by the approximation which completely neglected absorption. Only the asymmetry of a rocking curve and Borrmann effect are derived by the SIA theory with absorption taken into account.

If there is a X-ray source of tunable energy available, X-ray diffraction near the absorption edge of a constituent atom in the crystal, should be studied including the case of $f^0 > 0$, $f' < 0$, or $|f^0| \approx |f'|$. There are even the case that $f^0 + f' \leq 0$ or $|f^0 + f'| < |f''|$. In these cases, it will be difficult to interpret the dynamical diffraction by SIA.

1.2.3 Dispersion surface in two-wave approximation

The concept of the dispersion surface[6] is useful for explaining a dynamical theory and the diffraction phenomena. The dispersion-surface shows the relationship between the wave vectors and the frequencies of waves in the crystal. In the following paragraph we overview dispersion surfaces in two-wave approximation for understanding dynamical diffraction.

The interaction between X-rays and a crystal is well described by the so-called two-wave approximation. The cross section of the dispersion surface in this two-wave approximation is shown in Fig. 1.2. "O" is the origin of the reciprocal-lattice space which is taken as the end point of the incident wave vector in the crystal and "H" the relevant reciprocal-lattice point by one diffracted wave excited. When X-rays K_0 incident toward O from point N, tie points(A_1 , A_2 , B_1 and B_2) are intersection between the dispersion surface and a straight line ν perpendicular to the crystal surface which passes along N. When setting to K_0 and κ_0 the wave number of the X-rays under a vacuum and crystal, respectively, the relationship between K_0 and κ_0 is $\kappa_0 = n_0 K_0$ (n_0 : refractive-index, see 2.2.1). Two spheres with a radius of κ_0 , centering O and H are drawn. The intersection of

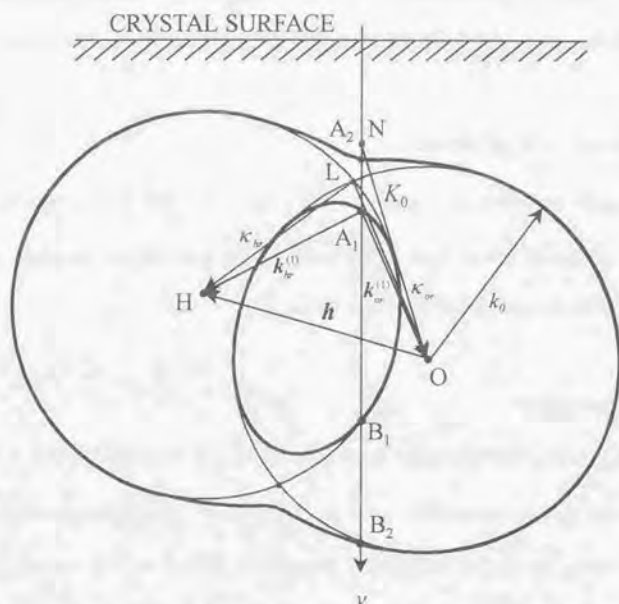


Fig. 1.2 The dispersion surface in two-wave approximation

two spheres satisfies exact Bragg conditions in which called Laue points L. In ordinary circumstances, since B_1 and B_2 are so far from L point, the excitation of the wave is very weak. Thus, two tie points, A_1 and A_2 are used. The waves toward O from two tie points correspond to transmitted waves($k_o^{(1)}, k_o^{(2)}$), and the waves toward H the diffracted waves($k_h^{(1)}, k_h^{(2)}$). In two-wave approximation, four waves exist in the crystal. In X-ray dynamical diffraction, the dispersion surface near point L is away from two spheres, and the interference effects among four waves is important. The distance from dispersion surface to spheres near point L about 10^{-6} and sections of the dispersion surface in the point L can be approximated by a straight line. In SIA, the dispersion surface is a

hyperbola, and the imaginary part of the dispersion surface is neglected. However, in this study, both the real part and imaginary part of the dispersion surface are important.

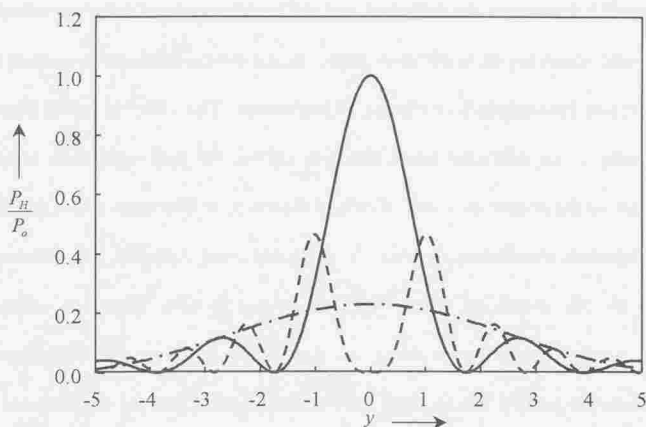
1.2.4 Wave Field in Crystal

In two-wave approximation, four waves, $k_o^{(1)}$, $k_o^{(2)}$, $k_h^{(1)}$ and $k_h^{(2)}$, exist in the crystal. A typical dynamical effect, such as the pendellösung beat and the standing wave are explained by the interference of these four waves.

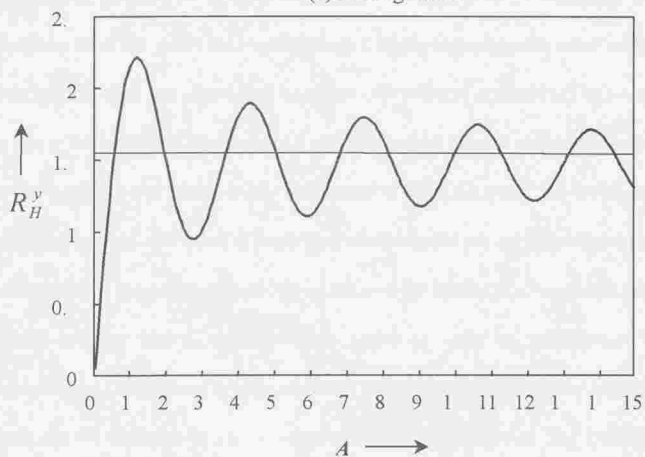
(i) Pendellösung beat

The pendellösung beat is induced by interference of two wave of $k_o^{(1)}$ and $k_o^{(2)}$ which are connected with the transmitted waves, or $k_h^{(1)}$ and $k_h^{(2)}$ which are connected with the diffracted waves, among waves from two tie points in the crystal. The rocking curve and the integrated reflecting powers which were obtained by Zachariasen [9] are shown in Fig1.3. These are calculated results in Laue case without absorption. (a) is a rocking curve obtained by carrying out small rotation of the diffraction angle near the Bragg angle. On the other hand (b) is an integrated reflecting power of the diffracted wave. The scale of abscissas is proportional to the crystal thickness. The increase and decrease in intensity of (a) and (b) are pendellösung beats.

In the study of X-ray diffraction, Kato and Lang (1959) [10] observed this (b) type pendellösung beat in the first. They found this pendellösung beat on a photograph of the Lang camera using a Si single crystal of the wedge form whose crystal thickness continuously changed. Then, (a) type pendellösung beats have been observed parallel with performance enhancement of the crystal monochromator.



(a) Rocking curve.



(b) Integrated reflecting powers as function of A

Fig.1.3 Pendellösung beat in the Laue case.[9]

(ii) Borrmann effect and standing waves in crystal

Borrmann [1] discovered the diffracted and the transmitted intensities by transmission through crystal which are 10 to 20 times thicker than a crystal thickness forecasted by the mean absorption (anomalous-transmission phenomenon). This effect is called *Borrmann effect*. Usually, if the diffracted beam becomes strong, the part transmitted beam will become weak by the conservation law of energy. However, in Borrmann effect, transmitted beam also increases simultaneously when the diffracted beam increases. This effect cannot be interpreted by the dynamical theory without absorption. The Borrmann effect was interpreted as follows by SIA with absorption. Among two tie points, the absorption of the wave from one tie point is smaller than the mean absorption, and the wave carries out an anomalous transmission. However, the wave from another tie point is absorbed greatly more than the mean absorption (anomalous absorption). This effect has been analyzed from the standpoint of the standing wave in the crystal by Batterman and Cole (BC) (1964) [11]. BC carried out the study for the wave field which synthesized the diffracted wave and the transmitted waves for every tie point in the crystal. As a result, two standing waves with the lattice period could be obtained, the one wave is known to have antinodes on the lattice plane and another is nodes. Consequently, waves with antinodes on the lattice plane decreased remarkably as they penetrate deep through crystal surface (anomalous absorption) and waves with nodes do not decrease almost (anomalous transmission). The Borrmann effect will be analyzed from the imaginary part of solutions for the dispersion surface in this paper.

1. 3 X-ray Resonance Scattering and Anomalous-Scattering Factor

In this section, anomalous scattering factors which estimate the scattering intensity for the study of the dynamical diffraction with the X-ray resonance scattering is described from the side of a classic theory. In this paper, atomic unit ($\hbar = m = e = 1$) is used for

simplified expression of the formula.

Let us assume that the electron for the scattering is bound to a nucleus by energy ω_s . When the electron carries out the forced oscillation by the electric field ($E_i = E_0 e^{i\omega t}$) of the incident beam. In point A which R apart from the electron, electric-field E' of the X-rays

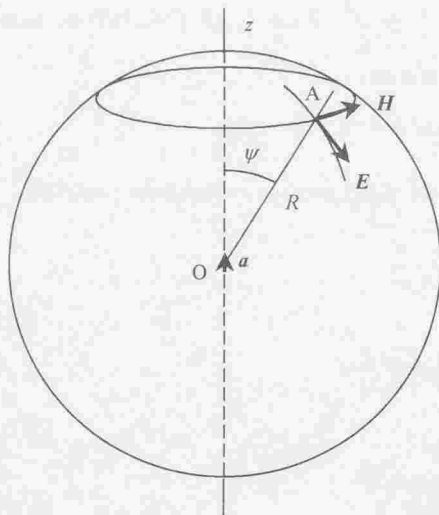


Fig 1.4. The electromagnetic field with the accelerating electron.

emitted from the electron is shown by the following equation(see Fig1.4)

$$|E'| = c^{-2} \frac{\sin \varphi}{R} |\ddot{r}| \quad (1.5)$$

Where, c is the velocity of light and r is the position of an oscillating electron. In (1.5), if the acceleration(\ddot{r}) of the electron caused by E_i is obtained, the intensity of the scattering X-rays can be calculated. Then, the displacement is examined. In Fig 1.4, the equation of motion for the electron in points O is given by the following(James [12])

$$\ddot{r} + k_d \dot{r} + \omega_s^2 r = -E_0 e^{i\omega t} \quad (1.6)$$

The solution of (1.6) is given by

$$\mathbf{r} = \frac{1}{\omega^2} \cdot \frac{\omega^2}{\omega^2 - \omega_s^2 - ik_d\omega} E_0 e^{i\omega t} \quad (1.7)$$

Where, k_d is the radiation damping factor caused by emission of the electromagnetic waves, and has the relationship as follows: $k_d = 2\omega^2(3c^3)^{-1}$. If the scattering is due to free electrons, $\mathbf{r}_{free} = \omega^{-2} E_0 e^{i\omega t}$ by $\omega_s = 0$ and $k_d = 0$. From (1.7), the relationship between free and bound electrons is given by

$$\mathbf{r} = \mathbf{r}_{free} \cdot f(\omega) = \mathbf{r}_{free} [f_r(\omega) + if_i(\omega)] \quad (1.8)$$

Where, $f(\omega)$, $f_r(\omega)$ and $f_i(\omega)$ are given by the following equations

$$f(\omega) = \frac{\omega^2}{\omega^2 - \omega_s^2 - ik_d\omega} \quad (1.9a)$$

$$f_r(\omega) = \frac{\omega^2(\omega^2 - \omega_s^2)}{(\omega^2 - \omega_s^2)^2 + k_d^2\omega^2} \quad (1.9b)$$

$$f_i(\omega) = \frac{k_d\omega^3}{(\omega^2 - \omega_s^2)^2 + k_d^2\omega^2} \quad (1.9c)$$

However, in actual atoms, it is not observed $f(\omega)$ as the large value which is calculated by the (1.9). For this reason, $f(\omega)$ for actual atoms is estimated by optical examination.

Let us the dipole momentum per oscillating electron is p , the relationship of $p = -r$ will be result. The permittivity $\varepsilon(\omega)$ becomes as follows

$$\varepsilon(\omega) = 1 + \frac{4\pi Np}{E_i} = 1 - \frac{4\pi Nf(\omega)}{\omega^2} \quad (1.10)$$

Where, N is the number of electrons in unit volume under the same conditions. Since the relationship of $n(\omega) = \sqrt{\varepsilon(\omega)}$ exists between refractive index $n(\omega)$ and $\varepsilon(\omega)$,

$n(\omega)$ is given by

$$n(\omega) = 1 - \alpha(\omega) - i\beta(\omega) \quad (1.11)$$

Where, $\alpha(\omega)$ and $\beta(\omega)$ are approximated as follows

$$\alpha(\omega) = \frac{2\pi N f_r(\omega)}{\omega^2} \quad (1.12a)$$

$$\beta(\omega) = \frac{2\pi N f_i(\omega)}{\omega^2} \quad (1.12b)$$

Since $\alpha(\omega)$ and $\beta(\omega)$ are obtainable from measurement of the reflectivity by the X-ray mirror, $f_r(\omega)$ and $f_i(\omega)$ are calculated from the relationship of (1.12). Thus, $f(\omega)$ of the boundary electron can be calculated.

On the other hand, the following relationship exists between the linear absorption coefficient $\mu_0(\omega)$ and the refractive index $n(\omega)$

$$\mu_0(\omega) = -\frac{2\omega}{c} \text{Im}\{n(\omega)\} = \frac{2\omega}{c} \beta(\omega) \quad (1.13)$$

Let us the absorption coefficient per one dipole to be $\mu(\omega)$, $f_i(\omega)$ will be given by

$$f_i(\omega) = \frac{c\omega}{4\pi} \mu(\omega) \quad (1.14)$$

Absorption of X-rays caused by mostly photoelectric effect and it is empirically known to become as shown in Fig.1.5. The absorption coefficient $\mu(\omega)$ has the maximum near ω_k and gradually becomes smaller when energy ω becomes larger than it. Given this experimental fact, the bound energy ω_k assumed in (1.6) is not discrete, and it is continuously. Therefore, the integral form is suitable for $f_r(\omega)$ and $f_i(\omega)$ as following([13]).

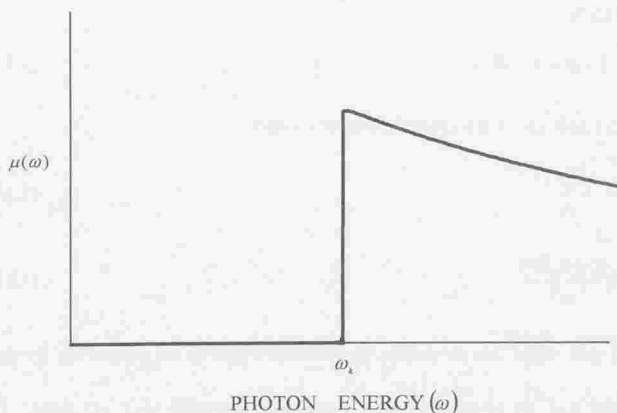


Fig 1.5. The linear absorption coefficient.

Assuming that the oscillator density between energy ω_s and $\omega_s + d\omega_s$ is $dg/d\omega_s$, $f_i(\omega)$ will be given as follows using (1.9c)

$$f_i(\omega) = \int \frac{(dg/d\omega_s)k_d\omega^3}{(\omega^2 - \omega_s^2)^2 + k_d^2\omega^2} d\omega_s \quad (1.15)$$

Assuming that the variation of $dg/d\omega_s$ is flatter than the Lorentz type function, the integration takes a value only near the $\omega_s \approx \omega$. Therefore (1.16) can be established

$$f_i(\omega) = \frac{\pi\omega}{2} \cdot \frac{dg}{d\omega} \quad (1.16)$$

However, when $dg/d\omega$ rises rapidly at an atom absorption edge, this approximation cannot be used. Based from $\mu(\omega)$ and (1.14), (1.17) can be obtained for $dg/d\omega$

$$\frac{dg}{d\omega} = \frac{c}{2\pi^2} \cdot \mu(\omega) \quad (1.17)$$

Therefore, if $\mu(\omega)$ is obtained by experimentally or theoretically, $dg/d\omega$ will be determined from (1.14). Similarly, $f_r(\omega)$ is calculated as follows using (1.9b)

$$f_r(\omega) = \int \frac{(dg/d\omega_s)\omega^2(\omega^2 - \omega_s^2)}{(\omega^2 - \omega_s^2)^2 + k_d^2\omega^2} d\omega_s \quad (1.18)$$

If $\mu(\omega)$ is decided, $dg/d\omega$ will be derived, and $f_r(\omega), f_i(\omega)$, namely, $f(\omega)$ can be calculated specifically.

The correspondence between $f(\omega)$ and anomalous-scattering factor is projected. Since f^0 becomes 1 from the hydrogen atom model for the forward scattering of X-rays, and $f(\omega)$ is written as follows

$$f(\omega) = f_r(\omega) + if_i(\omega) = 1 + f'(\omega) + if''(\omega) \quad (1.19)$$

Therefore, the following equation is obtained from (1.12), (1.15) and (1.16)

$$f'(\omega) = f_r(\omega) - 1 = \int \frac{(dg/d\omega_s)(\omega_s^2\omega^2 - \omega_s^4 - k_d^2\omega^2)}{(\omega^2 - \omega_s^2)^2 + k_d^2\omega^2} d\omega_s \quad (1.20a)$$

$$f''(\omega) = f_i(\omega) = \int \frac{(dg/d\omega_s)k_d\omega_s^3}{(\omega^2 - \omega_s^2)^2 + k_d^2\omega^2} d\omega_s \approx \frac{\pi\omega}{2} \cdot \frac{dg}{d\omega} \quad (1.20b)$$

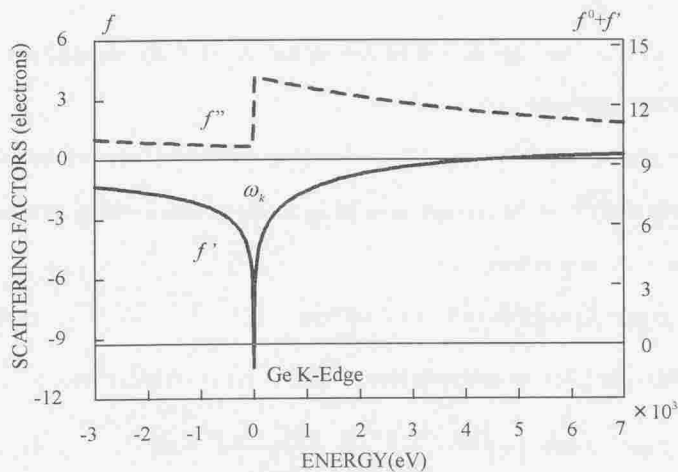
In order to derive (1.20 a), the sum rule of Thomas-Reich-Kuhn (TRK) was used as follow

$$\int (dg/d\omega_s) d\omega_s = 1. \quad (1.21)$$

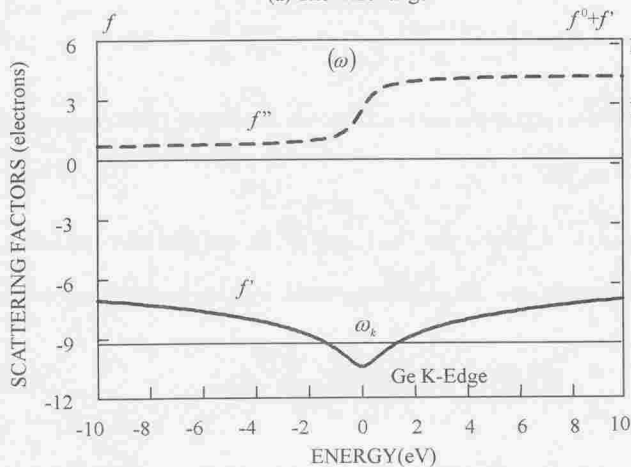
As follows, the dispersion of $f'(\omega)$ and $f''(\omega)$ are calculated. According to the experience, the photoelectric-absorption coefficient $\mu(\omega)$ can be approximated as follows

$$\begin{aligned} \mu(\omega) &= \mu_k \left(\frac{\omega_k}{\omega} \right)^{p_k}, & (\omega \geq \omega_k) \\ &= 0, & (\omega < \omega_k) \end{aligned} \quad (1.22)$$

Where, μ_k is the linear absorption coefficient at the absorption edge of energy ω_k , both p_k and μ_k will be determined in agreement with the measurement results.



(a) The wide range.



(b) The expansion of the near K-absorption edge.

Fig 1.6. The change of anomalous scattering factors, its real part $f(\omega)$ and its imaginary part $f''(\omega)$ of near the Ge K-absorption edge.

Therefore $dg/d\omega$ is given by

$$\frac{dg}{d\omega} = \frac{c}{2\pi^2} \mu_k \left(\frac{\omega_k}{\omega} \right)^{p_k} = g_k \left(\frac{\omega_k}{\omega} \right)^{p_k}, \quad (\omega \geq \omega_k) \quad (1.23)$$

Where, g_k accompanied by K -electrons is expressed in (1.24)

$$\begin{aligned} g_k &= \int_{\omega_k}^{\infty} \frac{dg}{d\omega} d\omega \\ &= g_k \int_{\omega_k}^{\infty} \left(\frac{\omega_k}{\omega} \right)^{p_k} d\omega = g_k \frac{\omega_k}{p_k - 1} \end{aligned} \quad (1.24)$$

Therefore, (1.25) is obtained

$$\frac{dg}{d\omega} = \frac{p_k - 1}{\omega_k} g_k \left(\frac{\omega_k}{\omega} \right)^{p_k}, \quad (\omega > \omega_k) \quad (1.25)$$

Approximating 1s electrons by $p_k = 2.75$, 2s by 2.33, and others by 2.5, Parratt and Hempstead(1954)[14] integrated (1.20a) and (1.20b), they derived the equation to calculate $f'(\omega)$ and $f''(\omega)$.

On the other hand, g_k is given by the TRK's sum rule for K -electron as follows

$$\int_{\omega_k}^{\infty} \frac{dg}{d\omega} d\omega + \sum_m g_m = g_k + \sum_m g_m = 2 \quad (1.26)$$

Here, $\sum_m g_m$ is calculated from the wave function of the ground state. If $\sum_m g_m$ is exactly obtained from a quantum theory, g_k is determined from an above(1.26). Cromer (1965) [15] obtained the wave function of the ground state by Hartree-Fock approximation, and calculated g_k for K, L and M, and presented a table of the result. Cromer showed simultaneously the table for f' and f'' of atoms to characteristic X-rays used in experiments, such as Cr K α , using the equation of Parratt and Hempstead. The dispersion at the absorption edge cannot be known from $f'(\omega)$ and $f''(\omega)$ calculated by Cromer. However, using Cromer's g_k and the equation of Parratt and Hempstead, $f'(\omega)$ and

$f''(\omega)$ in the absorption edge of arbitrary atoms is calculated. Fig 1.6 is shown $f'(\omega)$ and $f''(\omega)$ in K -absorption edge of germanium by using the method. (a) shows the wide energy range and (b) near the absorption edge. $f''(\omega)$ becomes large rapidly at the absorption edge in (a), it decreases gradually from the edge according to the high energy region. The dumping effect in the absorption edge is shown in (b). $f'(\omega)$ is always negative in the low energy region from the absorption edge and $f'(\omega) = -g_k$ at $\omega = 0$. In the absorption edge ($\omega_k = 11103.6\text{eV}$), $f'(\omega)$ is the smallest, it increase on the higher energy region than ω_k , becoming zero in the position about 1.5 times compared with ω_k , and becomes positive on the higher energy region than it. As shown in (b), in the range of $\pm 10\text{eV}$ of the absorption edge, both changes of $f'(\omega)$ and $f''(\omega)$ are intense, especially $f''(\omega)$ radically changes and $f'(\omega)$ becmes about -10 at an absorption edge.

Such dispersion is generated by the resonance scattering of the boundary electron. This effect appears most notably in the absorption edge and change most rapidly. Anomalous-scattering factors of this paper is obtained by the method using g_k of Cromer and the equation of Parratt and Hempstead.

In addition, Cromer and Liberman(1970)[16] calculated photoelectric-absorption μ by using the relativity, and gave the anomalous-scattering factor to characteristic X-rays in pure theory. They had been providing programs to calculate μ . By using these programs, Sasaki (1969)[17] had computed $f'(\omega)$ and $f''(\omega)$ for the wavelength from 0.10\AA to 2.89\AA , and reported the data table. However, since the table is no correction of dumping, the anomalous-scattering factor at the absorption edge is discontinuous. Therefore, this paper does not use Sasaki's table.

Kramers and Kronig's dispersion relation between $f'(\omega)$ and $f''(\omega)$ is calculated

from the following equation(1.27) using $f''(\omega)$

$$f'(\omega) = \frac{2}{\pi} \int \frac{f''(\omega_s) \omega_s}{\omega^2 - \omega_s^2} d\omega_s \quad (1.27)$$

Since $f''(\omega)$ is determined from $\mu(\omega_s)$, $f'(\omega)$ is calculated also from the dispersion relation of Kramers and Kronig. This relationship has been well established at present as the method to know $f'(\omega)$ from $f''(\omega)$ by XANES (X-ray Absorption Near Edge Structure).

1.4 Purpose of Study

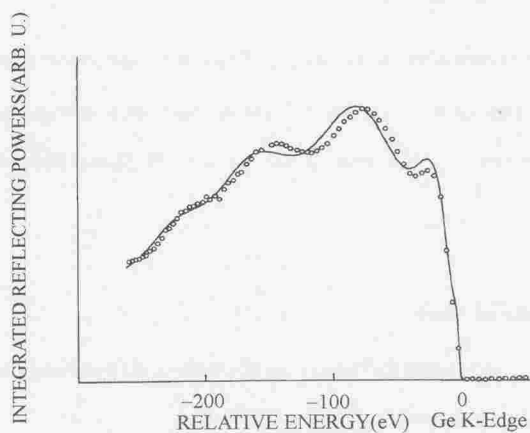
This section describes the background for this study of the dynamical theory with the X-ray resonance scattering and the purpose of this paper.

1.4.1 Observation of Pendellösung Beat with X-ray Resonance Scattering and Breakdown of SIA

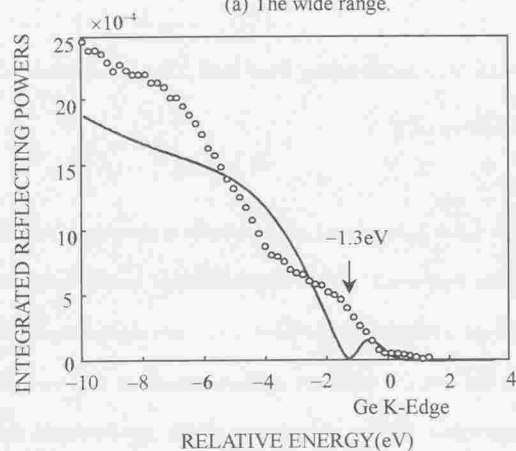
(i) Previous works

As described in 1-2-4(i), Kato and Lang succeeded in the observation of a pendellösung beat using a wedge type crystal whose thickness varied continuously. The pendellösung beat will be observed if the scattering cross section σ can change continuously by a certain method even if the crystal thickness is fixed. Based on this viewpoint, Takama *et al.*(1980)[18] succeeded in the observation of the pendellösung beat by changes wavelength continuously using the energy dispersive diffractometer with SSD(white X-rays pendellösung beat). Yoshizawa et al. (1988) [19], on the other hand, succeeded in the observation of the pendellösung beat just below Ga *K*-absorption edge of GaAs using the effect which shows the remarkable change of $f'(\omega)$ in the absorption edge, using the

energy dispersive diffractometer. The beat is called the pendellösung beat of an X-ray resonance scattering (PBXRS).



(a) The wide range.



(b) The expansion of the near K-absorption edge.

Fig 1.7. The integrated reflecting powers of Ge.

(ii) Present work

Authors (1993) [20] observed PBXRS of Ge 844 just below Ge K -absorption edge by using the synchrotron radiation and the energy dispersive diffractometer. A part of measurement results is shown in Fig.1.7. Open circles are the result of the measurement. (a) is shown over the wide energy range near the absorption edge. (b) shows the narrow range from -10eV to 4eV near the absorption edge. Solid lines are PBXRS which obtained from SIA theory. In this analysis, $f'(\omega)$ and $f''(\omega)$ were calculated by the method of Parratt and Hempstead shown in Fig.1.6. The solid line in Fig.1.7(a) well agree with the experimental results. However, in (b), the difference is seen clearly. Shoulder structures are looked at by the measured result at 2 places, -6eV and -2eV. The shoulder structure near -6eV is primary PBXRS. What is the shoulder structure near -2eV? The shoulder structure by PBXRS exists at about -4eV. And the solid line becomes zero at -1.3eV, and -0.8eV shows a small peak. As shown in Fig1.6, calculated results become zero at -1.3eV below Ge K -absorption edge with Ge 844 when $f^0 + f'$ changes from positive to negative. In case of Ge 844, f^0 takes the value of 9.24. On the other hand, f' varies from -7.06 to -9.26 when the relative energy changes from -10eV to -1.3eV below the absorption edge. Therefore, $|f^0 + f'|$ becomes almost zero at -1.3eV. $|f'|$ is larger than f^0 from -1.3eV to the absorption edge. The integrated reflecting powers by SIA has $|\chi_{hr}|$ in the coefficient. In case of Ge 844, if $f^0 + f'$ is zero, χ_{hr} is also zero. And, the integrated reflecting powers become zero. It is understood that integrated reflecting power of Ge 844 becomes zero at -1.3eV below the absorption edge. However, the experimental result is not zero. f'' is also not zero in the position at -1.3eV below the absorption edge in Fig1.6. When $|f^0 + f'|$ becomes zero, f'' is not zero, thus, it is very unnatural that integrated reflecting powers becomes zero. In the kinematical theory, f'' is not zero even when $f^0 + f'$

become zero, integrated reflecting powers is also not zero. Therefore the calculated result of integrated reflecting powers in Fig.1.7 is unnatural. Under these circumstances, the shoulder structure is judged to be the cause that $f^0 + f'$ becomes zero. However, SIA has inconsistency that a diffracted intensity becomes zero at $f^0 + f' = 0$. Therefore, a new dynamical theory which is also applicable to $f^0 + f' = 0$ is needed.

1.4.2 Circumstances of Study

In near the absorption edge, since $|f^0|$ and $|f'|$ become almost equal by high order reflection and $f^0 + f'$ become 0 as the result, it is shown that there is the dynamical diffraction only due to f'' . And, when $|f^0 + f'|$ became zero, integrated reflecting powers by SIA had inconsistency of becoming zero, regardless of f'' not being zero. For this reason, Fukamachi and Kawamura(1993) [21] (FK) derived a new theoretical formula which did not have to be approximated as SIA. And they examined some features of the dynamical diffraction only due to f'' . According to the result, in Bragg case of the semi-infinite crystal, the rocking curve of only f'' became sharper than the case of only $|f^0 + f'|$ (in addition, Kato (1992) [22] derived this effect theoretically). In Laue case, the anomalous transmission appeared in the rocking curve of only f'' even though crystal is thin, contrary to general expectation, the pendellösung beat could be noticed in the tail of rocking curves when the absorption is large. Authors[20] identified that the shoulder structure in the integrated reflecting powers below Ge *K*-absorption edge was based on $f^0 + f' = 0$ with the application using the theoretical formula of FK. Then, authors (1994) [23] examined the dynamical diffraction of Laue case in detail by changing the ratio of $|f^0 + f'|$ and $|f''|$. Consequently, the following effect appeared in the rocking curve of the

transmitted beam with the X-ray resonance scattering.

1. Existence of asymmetry,
2. Nontransparent effect to which X-ray do not penetrate thin crystal at all,
3. The unusual increase of anomalous transmission in asymmetrical reflection

In addition, authors (1995) [24] studied the dispersion surface by the FK method. In SIA, the solution in the dispersion surface used the real part, but the imaginary part used under the necessary. However when FK method is applied, the dispersion surfaces are complex numbers and that it is special cases that the dispersion surface becomes real number only. The shape of the dispersion surface also changed due to ratios between $|f^0 + f'|$ and $|f''|$ remarkably, the following phenomena have understood visually in case of f'' only. On one hand is the reason which the rocking curve in Bragg case with the semi-infinite crystal becomes sharp, on the other is the reason which both the diffracted and the transmitted beams in symmetrical Laue case carry out the anomalous transmission of the 25% of the incident beam.

Then, authors (1997) [25] examined the standing wave in the crystal studied by Batterman and Cole using FK method. The phase difference of $\pi/2$ in a standing waves are found out between the case of only $f^0 + f'$ and the case of only f'' . The cause of anomalous transmission in the symmetric Laue case was solved also from the standpoint of the standing wave.

The purpose of this study is to systematize the dynamical diffraction theory with the X-ray resonance scattering by FK method. This study also experimentally analyzes the appropriateness of this theory.

References

- [1] G. Borrmann(1941)"*Über Extinktionsdiagramme von Quarz*", *Phys. Z.*, **42**, 157-162.
G. Borrmann(1950)"*Die Absorption von Röntgenstrahlen im Fall der Interferenz*",
Phys. Z., **127**, 297-323.
- [2] W. Friedrich, P. Knipping, M. v. Laue(1912)"*Interferenzerscheinungen bei Röntgenstrahlen*", *Sitzungber. D. Bayer. Akademie der Wnssenschaften*, 303-322.
- [3] S. Miyake(1969)"*X-ray Diffraction*", Tokyo:Asakura(in Japanese).
- [4] C. G. Darwin(1914)"*The Theory of X-Ray Reflection*", *Phil. Mag.*, **27**, 315-333,
675-690.
- [5] C. G. Darwin(1922)"*The Reflection of X-Rays from Imperfect Crystals*", *Phil. Mag.*,
43, 800-829.
- [6] P. P. Ewald(1917)"*Die Kristalloptik der Röntgenstrahlen*", *Ann. Phys.*, **54**, 519-597.
- [7] M. v. Laue(1931)"*Die dynamische Theorie der Röntgenstrahlinterferenzen in neuer Form*", *Ergebnisse der Exakt. Naturwiss.*, **10**, 133-158.
- [8] N. Kato(1974),"X-Ray Dffraction"(ed. by L. V. Azárov), Chapter 4, Mcggraw-Hill,
New York.
- [9] for example: W. H. Zachariasen(1945)"*Theory of X-ray Diffraction in Crystals*",
New York:Dover.
- [10] N. Kato and A. R. Lang(1959)"*A Study of Pendellösung Fringes in X-ray Diffraction*", *Acta Cryst.*, **12**, 787-794.
- [11] B. W. Batterman, & H. Cole (1964)"*Dynamical Diffraction of X-rays by Perfect Crystals*", *Rev. Mod. Phys.*, **36**, 681-717.
- [12] R. W. James(1954)"*The Optical Principles of the Diffraction of X-Rays*", G.Bell and Sons.
- [13] T. Fukamachi(1977)"*Theoretical Survey of Anomalous Scattering Factors of X-Rays*", *J. Cryst. Soc. Jpn.*, **19**, 51-67(in Japanese).
- [14] L. G. Parratt and C. F. Hempstead(1954)"*Anomalous Dispersion and Scattering of*

X-Rays", *Phys. Rev.* **19**, 1593-1600.

- [15] D. T. Cromer(1965)"*Anomalous Dispersion Corrections Computed from Self-Consistent Field Relativistic Dirac-Slater Wave Functions*", *Acta Cryst.*, **18**, 17-23.
- [16] D. T. Cromer and J. Liberman(1970)"*Relativistic Calculation of Anomalous Scattering Factors for X Rays*", *J. Chem. Phys.* **53**, 1891-1898.
- [17] S. Sasaki(1989)"*Numerical Tables of Anomalous Scattering Factors Calculated by the Cromer and Liberman's Method*", KEK Report 88-14 M/D, 1-136.
- [18] T. Takama, M. Iwasaki and S. Sato(1980) , *Acta Cryst.*, **A36**, 1025-1030.
- [19] M. Yoshizawa, T. Fukamachi, K. Ehara, T. Kawamura and K. Hayakawa(1988) "*Observation of Pendellösung Fringes Induced by X-ray Resonant Scattering*", *Acta Cryst.*, **A44**, 433-436.
- [20] T. Fukamachi, R. Negishi, M. Yoshizawa, K. Ehara, T. Kawamura, T. Nakajima and Z. Zhao(1993)"*X-ray Dynamical Diffraction in Ge with a Zero-Real-Part Scattering Factor*", *Acta Cryst.*, **A59**, 573-575.
- [21] T. Fukamachi and T. Kawamura(1993)"*Xray Diffraction when the Real Part of the Scattering Factor is Zero*", *Acta Cryst.*, **A49**, 384-388.
- [22] N. Kato(1992)"*A Note on the Darwin-Prins Rocking Curve for Perfect Crystals*", *Acta Cryst.*, **A48**, 829-834.
- [23] T. Fukamachi, R. Negishi and T.Kawamura(1994)"*Dynamical Diffraction in the Laue Case with Borrmann Absorption*", *Acta Cryst.*, **A50**, 475-480.
- [24] T. Fukamachi, R. Negishi and T. Kawamura(1995)"*The Dispersion Surface of X-rays Very Near the Absorption Edge*", *Acta Cryst.*, **A51**, 253-258.
- [25] R. Negishi, T. Fukamachi and T. Kawamura(1997)"*X-ray Standing Wave only due to Imaginary Part of Atomic Scattering Factor*", *Acta Cryst.*,(to be published).

1. The first step in the process of developing a business plan is to conduct a market analysis. This involves researching the industry, identifying potential customers, and understanding the competitive landscape.

2. The second step is to develop a marketing strategy. This includes determining how to reach potential customers, what promotional activities to undertake, and how to measure the effectiveness of the marketing efforts.

3. The third step is to create a financial plan. This involves estimating the costs of the business, projecting revenue, and determining the break-even point. It also includes developing a budget and identifying sources of funding.

4. The fourth step is to write a business plan. This document should outline the business's goals, strategies, and financial projections. It should also include a description of the business and its market.

5. The fifth step is to present the business plan to potential investors or lenders. This involves making a pitch and providing supporting documentation. It is important to be prepared to answer questions and address concerns.

6. The sixth step is to implement the business plan. This involves putting the strategies and financial projections into action. It is important to monitor progress and make adjustments as needed.

7. The seventh step is to evaluate the business plan. This involves assessing the results of the business and determining whether the plan is working. It is important to be flexible and willing to make changes.

CHAPTER II DYNAMICAL THEORY WITH RESONANCE SCATTERING

In this chapter, the general formulae of a dynamical theory are presented. They successfully deal with the scattering factor of the constituting atom, which has a larger value of the imaginary part comparing with that of the real part. The dynamical theory with small absorption of Miyake (1969) [1] was taken as reference for developing theory in this paper.

2.1. Fundamental Equations

2.1.1 X-Ray Electric Susceptibility without Absorption

Miyake's theory treats at first the perfect crystal which does not have disorder in the 3-dimensional lattice at all. It assumes that the following Maxwell's equation about the electromagnetic field in a vacuum also satisfies to the electromagnetic field in the crystal

$$\text{rot } \mathbf{H} = \frac{1}{c} \left[\frac{\partial \mathbf{E}}{\partial t} + 4\pi \mathbf{j}(\mathbf{r}) \right]. \quad (2.1)$$

Since the forced oscillation of electrons bound to a nucleus by incident X-rays $\mathbf{E}(\mathbf{r}, \omega) = E_0 e^{2\pi i(\omega t - \mathbf{k} \cdot \mathbf{r})}$, current density $\mathbf{j}(\mathbf{r})$ can be expressed by the sum of $\mathbf{j}_1(\mathbf{r})$, by Thomson scattering, and $\mathbf{j}_2(\mathbf{r})$, by the X-ray resonance scattering[2]

$$\mathbf{j}(\mathbf{r}) = \mathbf{j}_1(\mathbf{r}) + \mathbf{j}_2(\mathbf{r}). \quad (2.2)$$

In the case of $\omega_s \ll \omega$ (see 1.3), where an X-ray resonance scattering can be neglected in the equation of motion for electron, electrons are approximated as free electrons. (2.3) is derived from the equation(1.6) of Chapter I

$$\ddot{\mathbf{r}} = -\mathbf{E}. \quad (2.3)$$

Since \mathbf{r} changes including $e^{i\omega t}$ as in \mathbf{E} , $\dot{\mathbf{r}}$ is given by the following equation

$$\dot{\mathbf{r}} = \frac{\dot{\mathbf{E}}}{\omega^2}. \quad (2.4)$$

By multiplying the electron density $\rho(\mathbf{r})$ a certain place in a crystal to (2.4), the current density $\mathbf{j}_1(\mathbf{r})$ of the place will be given by the following equation

$$\mathbf{j}_1(\mathbf{r}) = -\frac{\rho(\mathbf{r})}{\omega^2} \frac{\partial \mathbf{E}}{\partial t}. \quad (2.5)$$

Substituting $\mathbf{j}_1(\mathbf{r})$ in one of Maxwell's equation (2.1), (2.6) establishes

$$\text{rot } \mathbf{H} = \frac{1}{c} \left[1 - \frac{4\pi}{\omega^2} \rho(\mathbf{r}) \right] \frac{\partial \mathbf{E}}{\partial t}. \quad (2.6)$$

$\varepsilon(\mathbf{r})$ is defined as follows

$$\varepsilon(\mathbf{r}) = 1 - \frac{4\pi}{\omega^2} \rho(\mathbf{r}). \quad (2.7)$$

Moreover, the following formula is introduced

$$\mathbf{D} = \varepsilon \mathbf{E}. \quad (2.8)$$

The \mathbf{D} corresponds to the electric displacement in a usual medium including change of local \mathbf{r} and time. Then, the \mathbf{D} is called electric displacement for convenience henceforth. Equation (2.6) is written as follows

$$\text{rot } \mathbf{H} = \frac{1}{c} \frac{\partial \mathbf{D}}{\partial t}. \quad (2.9)$$

Since we consider only the relation between time change partial in an action of incidence X-rays, Maxwell's equation of the following satisfies them.

$$\text{div } \mathbf{D} = 0, \quad (2.10a)$$

$$\text{rot } \mathbf{E} = -\frac{1}{c} \frac{\partial \mathbf{H}}{\partial t}, \quad (2.10b)$$

$$\text{div } \mathbf{H} = 0. \quad (2.10c)$$

These are the same forms as Maxwell's equation to the dielectric whose permittivity is $\varepsilon(\mathbf{r})$. However, $\varepsilon(\mathbf{r})$ is a local quantity defined by (2.7) and is the quantity with the same said also of E and j .

Since $\rho(\mathbf{r})$ is quantity depends on \mathbf{r} locally in an X-ray domain, $\varepsilon(\mathbf{r})$ also serves as the function of \mathbf{r} again. Since $\varepsilon(\mathbf{r})$ is very close to 1, it sets as follows

$$\varepsilon(\mathbf{r}) = 1 + \chi(\mathbf{r}). \quad (2.11)$$

Therefore $\chi(\mathbf{r})$ is as follows from (2.7)

$$\chi(\mathbf{r}) = -\frac{4\pi}{\omega^2} \rho(\mathbf{r}). \quad (2.12)$$

$\chi(\mathbf{r})$ is 4π times the electric susceptibility, this is called X-ray electric susceptibility.

In a crystal, the following relationship [3] exists between crystal structure factors F_h and $\rho(\mathbf{r})$ [3]

$$\rho(\mathbf{r}) = \frac{1}{v_c} \sum_h F_h \exp[-2\pi i(\mathbf{h} \cdot \mathbf{r})]. \quad (2.13)$$

Where, v_c is the volume of a unit cell. In a crystal, $\rho(\mathbf{r})$ is a periodic function with a lattice period, $\chi(\mathbf{r})$ also has a lattice period. Therefore, $\chi(\mathbf{r})$ is expanded by a Fourier series as in the following

$$\chi(\mathbf{r}) = \sum_h \chi_h \exp[-2\pi i(\mathbf{h} \cdot \mathbf{r})]. \quad (2.14)$$

The coefficient F_h on the right-hand side of (2.13) carries out Fourier conversion of the $\rho(\mathbf{r})$, and is given by the following

$$F_h = \int_{\text{unit cell}} \rho(\mathbf{r}) \exp[2\pi i(\mathbf{h} \cdot \mathbf{r})] d\mathbf{v}. \quad (2.15)$$

$\chi(\mathbf{r})$ of (2.14) is given by the following equation of the same method

$$\begin{aligned}\chi_h &= \frac{1}{V_c} \int_{\text{unit cell}} \chi(\mathbf{r}) \exp[2\pi i(\mathbf{h} \cdot \mathbf{r})] d\mathbf{r} \\ &= -\frac{4\pi}{V_c \omega^2} F_h\end{aligned}\quad (2.16)$$

(2.16) gives between χ_h and F_h . On the other hand, F_h is given by the following equation

$$F_h = \sum_j f_j^0(\mathbf{h}) \exp[2\pi i(\mathbf{h} \cdot \mathbf{r})]. \quad (2.17)$$

In this equation, f_j^0 is a normal atomic scattering factor of j -th.

2.1.2 X-Ray Electric Susceptibility with Absorption

If the energy of incident X-rays is near to the absorption edge of the constituting atom in a crystal, the resonance scattering by the electron bound to the nucleus cannot neglect.

In this case, as already discussed in Chapter I, the magnitude of $j_2(\mathbf{r})$ in (2.1) will become roughly equal to $j_1(\mathbf{r})$. $\varepsilon(\mathbf{r})$ is given by the complex number as (1.7) in Chapter I. For this reason, $\chi(\mathbf{r})$ is also a complex number. Assuming a real part and a imaginary part of $\chi(\mathbf{r})$ also to be $\chi_r(\mathbf{r})$ and $\chi_i(\mathbf{r})$, $\chi(\mathbf{r})$ is given by the following

$$\chi(\mathbf{r}) = \chi_r(\mathbf{r}) + i\chi_i(\mathbf{r}). \quad (2.18)$$

$\chi_r(\mathbf{r})$ and $\chi_i(\mathbf{r})$ of (2.18) are given as follows by the same method as (2.14)

$$\chi_r(\mathbf{r}) = \sum_h \chi_{hr} \exp[-2\pi i(\mathbf{h} \cdot \mathbf{r})], \quad (2.19a)$$

$$\chi_i(\mathbf{r}) = \sum_h \chi_{hi} \exp[-2\pi i(\mathbf{h} \cdot \mathbf{r})]. \quad (2.19b)$$

By analogy of (2.15) and (2.17), χ_{hr} and χ_{hi} of (2.19) are obtained as following equations

$$\chi_{hr} = -\frac{4\pi}{V_c \omega^2} \sum_j [f_j^0(\mathbf{h}) + f_j'(\omega)] \exp[2\pi i(\mathbf{h} \cdot \mathbf{r}_j)] \cdot T_j, \quad (2.20a)$$

$$\chi_{hi} = -\frac{4\pi}{v_c \omega^2} \sum_j [f_j''(\omega)] \exp[2\pi i(\mathbf{h} \cdot \mathbf{r}_j)] \cdot T_j. \quad (2.20b)$$

Thus, χ_{hr} is expressed with $f'' + f'$ and χ_{hi} is expressed with f'' . T_j is a correction term of temperature and \sum means the sum of the atom in the unit cell.

Both χ_{hr} and χ_{hi} in (2.19) are complex numbers and can be expressed as the following relationship

$$\chi_{hr} = |\chi_{hr}| \exp(i\alpha_{hr}), \quad (2.21a)$$

$$\chi_{hi} = |\chi_{hi}| \exp(i\alpha_{hi}). \quad (2.21b)$$

2.1.3 Fundamental Equations

From the Maxwell's equation to the electromagnetic field in a crystal, the fundamental equation of dynamical-diffraction theory is drawn as follows[1]

$$\frac{k_h^2 - K_0^2}{k_h^2} D_h = \chi_{h-g} D_{g[\perp k_h]}. \quad (2.22)$$

Here

$$\mathbf{k}_h = \mathbf{k}_0 + \mathbf{h}, \quad (2.23)$$

and, $\mathbf{k}_h, \mathbf{k}_0$ are the h -th and 0-th wave-number vector in the crystal. K_0 is the wave number of the wave in a vacuum. \mathbf{g} is a reciprocal-lattice vector except \mathbf{h} points. χ_{h-g} are the h - g order Fourier coefficient of $\chi(\mathbf{r})$. D_h and D_g are \mathbf{h} of $D(\mathbf{r})$ and the g -th Fourier coefficient. And $D_{g[\perp k_h]}$ is a component perpendicular to \mathbf{k}_h of D_g .

In a dynamical theory, the number of fundamental equations are n when n waves exists in the crystal, when there are n fundamental equations. In order to obtain a solution, n simultaneous equations containing \mathbf{h} and \mathbf{g} are solved.

2.2. Solutions of Fundamental-Equations

In this section, (2.22) is solved under specific boundary conditions. When only one wave k_o propagate in a crystal, the situation is called *one-wave approximation*, when two waves of k_o and k_h propagate in the crystal, the case is called *two-wave approximation*.

2.2.1 One-Wave Approximation

When only one wave k_o exists in the crystal, (2.22) is given by the following equation

$$(k_o^2 - K_o^2)D_o = k_o^2 \chi_o D_o. \quad (2.24)$$

The following is obtained from (2.24)

$$k_o^2 = \frac{K_o^2}{1 - \chi_o}. \quad (2.25)$$

Let's define the quantity κ_o as $\kappa_o = |k_o|$. (2.25) has the following relation to refractive-index n_o of X-rays as follows

$$n_o = \frac{|k_o|}{|K_o|} = \frac{\kappa_o}{K_o} = \frac{1}{\sqrt{1 - \chi_o}}. \quad (2.26)$$

Since χ_o is almost negative real number of the order of 10^{-6} , n_o is slightly smaller than 1, n_o and κ_o are given by the following equation from (2.26), respectively

$$n_o = 1 + \frac{1}{2} \chi_o = 1 + \frac{1}{2} \chi_{or} + i \frac{1}{2} \chi_{oi}, \quad (2.27)$$

$$\kappa_o = K_o \left(1 + \frac{1}{2} \chi_o\right) = \kappa_{or} + i \kappa_{oi}. \quad (2.28)$$

Therefore, κ_{or} and κ_{oi} are as follows

$$\kappa_{0r} = K_0 \left(1 + \frac{1}{2} \chi_{0r}\right), \quad (2.29a)$$

$$\kappa_{0i} = \frac{1}{2} K_0 \chi_{0i} \equiv \frac{1}{2} \kappa_{0r} \chi_{0i}. \quad (2.29b)$$

χ_{0r} and χ_{0i} are given by the following equation from (2.17)

$$\chi_{0r} = -\frac{4\pi}{v_c \omega^2} \sum_j [Z + f'(\omega)]_j, \quad (2.30a)$$

$$\chi_{0i} = -\frac{4\pi}{v_c \omega^2} \sum_j f_j''(\omega). \quad (2.30b)$$

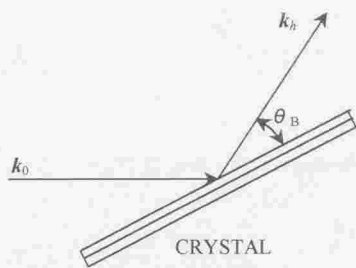
Here Z is the atomic number. The χ_{0i} becomes liner absorption coefficient μ_0 shown by (1.13) of Chapter I, and the following relation.

$$\mu_0 = -2\pi K_0 \chi_{0i}. \quad (2.31)$$

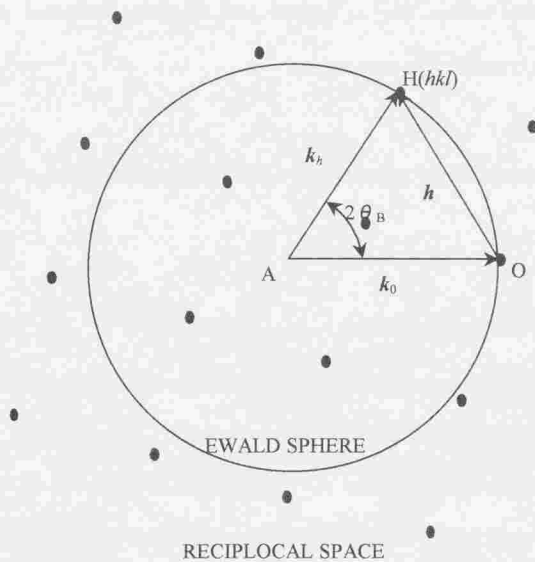
Therefore, when the resonance scattering exists, there is always absorption of the X-rays by the crystal.

2.2.2 Two-Wave Approximation

In this section, it is discussed that one diffracted wave k_h exists in a crystal as well as the k_0 which is very similar to incident rays K_0 (see Fig. 2.1(a)). The diffraction condition is understood by the Ewald construction of Fig. 2.1(b): The starting point of the vector k_0 which goes to origin O is tie point A (Ausbreitungspunkt). We name Ewald sphere the sphere of the radius AO centering around point A. When reciprocal-lattice point H lies on Ewald sphere, the diffracted wave of vector $\overline{AH} = k_h$ arises.



(a) Diffraction



(b) Ewald construction

Fig. 2.1 The Ewald construction

(i) Solution of two-wave approximation

The related equation which specifies the position of the tie point in reciprocal-lattice space is drawn from the fundamental equation (2.22). As for two-wave approximation, k_o and k_h are excited in a crystal. Let $D_{o\perp}$ and $D_{h\perp}$ be the perpendicular components (σ -polarization) to be plane of k_o and k_h of D_o and D_h . Similarly, $D_{o\parallel}$ and $D_{h\parallel}$ be the parallel components (π -polarization). The fundamental equation (2.22) is written by the following equation.

σ -component :

$$\frac{k_o^2 - \kappa_o^2}{k_o^2} D_{o\perp} = \chi_{-h} D_{h\perp}, \quad (2.32a)$$

$$\frac{k_h^2 - \kappa_o^2}{k_h^2} D_{h\perp} = \chi_h D_{o\perp}. \quad (2.32b)$$

π -component :

$$\frac{k_o^2 - \kappa_o^2}{k_o^2} D_{o\parallel} = \chi_{-h} \cos 2\theta_B D_{h\parallel}, \quad (2.33a)$$

$$\frac{k_h^2 - \kappa_o^2}{k_h^2} D_{h\parallel} = \chi_h \cos 2\theta_B D_{o\parallel}. \quad (2.33b)$$

Where $2\theta_B$ is an angle between k_o and k_h . In order to simplify expression of formula, ξ_o and ξ_h of the following are introduced

$$k_o - \kappa_{or} = \xi_o, \quad (2.34a)$$

$$k_h - \kappa_{or} = \xi_h. \quad (2.34b)$$

In order to exist the non-trivial solution for the simultaneous equations of (2.32) and (2.33), the following equation must be satisfied

$$\left| \frac{k_o^2 - \kappa_o^2}{k_o^2} \frac{P\chi_{-h}}{P\chi_h} \right| = 0, \quad (2.35a)$$

where, polarization factor P takes one of the alternative values of 1(σ -polarization) and $\cos 2\theta_B$ (π -polarization). Since terms of the equal to or more than 2nd order of ξ_o/κ_{or} and ξ_h/κ_{or} are negligibly, (2.35a) becomes

$$(\xi_o - i\kappa_{oi})(\xi_h - i\kappa_{oi}) = \frac{1}{4}\kappa_{or}^2 P^2 \chi_h \chi_{-h}. \quad (2.35b)$$

(ii) When there is no absorption

In this section, symmetrical reflection is examined. When there is no absorption, $\chi_{oi} = 0$ from (2.31), and $\kappa_{oi} = 0$ from (2.29). Therefore, (2.35b) becomes as

$$\xi_o \xi_h = \frac{1}{4}\kappa_{or}^2 P^2 \chi_h \chi_{-h}. \quad (2.36)$$

ξ_o and ξ_h in symmetrical reflection are given by the following, and ξ_o and ξ_h of this formula are shown in Fig. 2.2

$$\xi_o = Y' \sin \theta_B + X' \cos \theta_B, \quad (2.37a)$$

$$\xi_h = X' \cos \theta_B - Y' \sin \theta_B. \quad (2.37b)$$

Here, X' and Y' are bisectors of PP' and QQ' . Substituting ξ_o and ξ_h into (2.35b), a following equation is obtained

$$X' \cos^2 \theta_B - Y' \sin^2 \theta_B = \frac{1}{4}\kappa_{or}^2 P^2 \chi_h \chi_{-h}. \quad (2.38)$$

In Fig. 2.2, the cross section of the dispersion surface (2.38) in OHL is a hyperbola with two asymptotic lines (PP' and QQ'). Here, we will consider $\chi_h \chi_{-h}$ without the absorption when

$f''=0$. In this case, $j_2(\mathbf{r})$ of (2.1) is neglected and χ_i will be given by (2.13). Therefore,

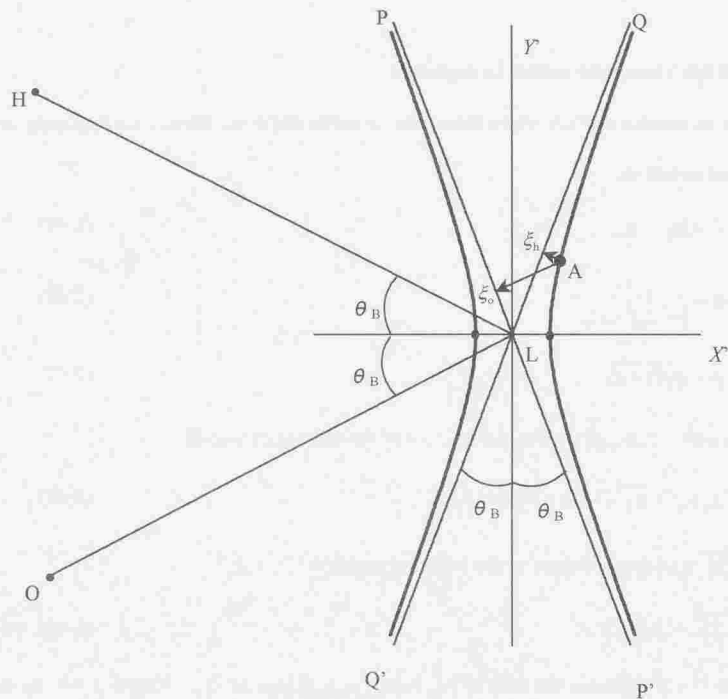


Fig.2.2 Tie points on the dispersion surface near the Laue point(L)

(2.39) will establish

$$\chi_h \chi_{-h} = \left(\frac{4\pi}{v_g \omega^2} \right)^2 F_h F_{-h} \quad (2.39)$$

Generally, F_h is a complex number, if F_{hr} and F_{hi} express the real and the imaginary parts of F_h , respectively, and $\chi_h \chi_{-h}$ is given by the following equation as a positive real number

$$\chi_h \chi_{-h} = \left(\frac{4\pi}{v_e \omega^2} \right)^2 (F_{hr}^2 + F_{hi}^2) \quad (2.40)$$

(iii) When absorption cannot be neglected

Let us examine the case where absorption cannot be neglected. Parameters δ , q , and p are defined as follows

$$\delta = \alpha_{hi} - \alpha_{hr}, \quad (2.41)$$

$$q = \frac{1}{1 + |\chi_{hr}|^2 / |\chi_{hi}|^2}, \quad (2.42)$$

$$p = \sqrt{q(1-q)}. \quad (2.43)$$

As a result, $\chi_h \chi_{-h}$ of (2.35b) will be given by the following equation

$$\chi_h \chi_{-h} = \overline{\chi_h}^2 (1 - 2q + 2ip \cos \delta) \quad (2.44)$$

This $\overline{\chi_h}^2$ (2.44) was defined by the following equation

$$\overline{\chi_h}^2 = |\chi_{hr}|^2 + |\chi_{hi}|^2. \quad (2.45)$$

q in (2.42) expresses the ratio of $|\chi_{hr}|$ and $|\chi_{hi}|$. In case of $\chi_{hi} = 0$, $q = p = 0$. In the case of $|\chi_{hr}| = |\chi_{hi}|$, $q = p = 0.5$. And, in the case of $\chi_{hr} = 0$, $p = 0$ and $q = 1$. Therefore, the range of q is 0 to 1. q approaches from 0 to 1 as the amplitude of χ_{hi} increases from 0.

These relationship decided by the ratio of $|\chi_{hr}|$ and $|\chi_{hi}|$ is shown in Table 2.1.

Table 2.1

	q	p	$1 - 2q$	$\chi_h \chi_{-h}$
(1) $\chi_{hi} = 0$	0	0	1	$ \chi_{hr} ^2$
(2) $ \chi_{hr} = \chi_{hi} $	0.5	0.5	0	$i \overline{\chi_h}^2 \cos \delta$
(3) $\chi_{hr} = 0$	1	0	-1	$- \chi_{hi} ^2$

As shown in the table, $\chi_h \chi_{-h}$ of (2.44) is the positive real number in $q=0$. However in $q=1$, $\chi_h \chi_{-h}$ is the negative real number conversely. In $q=0.5$, $\chi_h \chi_{-h}$ is a pure imaginary number. In the other case of q , $\chi_h \chi_{-h}$ is a complex number.

(iv) Equation of the dispersion surface

(2.35b) is an equation which specifies the dispersion surface of the reciprocal-lattice space with a resonance scattering. The following quantities are shown in Fig. 2.3.: tie points on the dispersion surface, the orientation of the crystal surfaces, Laue point, Bragg angle and other orientation relations. The diagram is the cross section of the real part of the dispersion surface of Laue case. ξ_o and ξ_h are far smaller than compared with the radius $|\kappa_o|$ of two spheres (about 10^{-5} to 10^{-6}). For this reason, the cross section of the sphere near the intersection L of two spheres is approximated in straight lines. Similarly, the cross section of the dispersion surface is approximated by a hyperbola. Each tie point is distinguished by suffix of 1 and 2 as shown in the figure.

When X-rays K_o incident toward O from point N, tie points are intersections between the dispersion surface and a straight line ν perpendicular to the crystal surface which passes along N. θ_B is Bragg angle. Axis X is parallel to the crystal surface and axis Y is perpendicular to axis X . The distance ξ_o and ξ_h between tie points and the asymptotic lines are given by

$$\xi_o = X \sin \theta_1 + Y \cos \theta_1, \quad (2.45a)$$

$$\xi_h = X \sin \theta_2 + Y \cos \theta_2. \quad (2.45b)$$

When X and Y are coordinates of tie point A. Refer to Fig. 2.3 regarding θ_1 and θ_2 . (2.35b) will become as follows by substituting the relationship of (2.45)

$$\begin{aligned}
& X^2 \sin \theta_1 \sin \theta_2 + Y^2 \cos \theta_1 \cos \theta_2 + XY \sin 2\beta \\
& - 2i\kappa_{oi} \cos \theta_B (X \cos \beta + Y \sin \beta) - \kappa_{oi}^2 \\
& = \frac{1}{4} \kappa_{or}^2 \chi_h^{-2} (1 - 2q + 2ip \cos \delta)
\end{aligned} \quad (2.46)$$

(2.46) is an equation of the dispersion surface with a resonance scattering. The solutions X and Y may be the complex number. However, I found that X is safely defined to be a real-number variable. This notion is very useful tool for interpret all of experiment, because the direction of the incident X-ray is most simply represented by real number of X . Setting complex-number $Y=Y+iZ$ (Y, Z both real number)[7]. The real part and the imaginary one of (2.46) are separately as follows.

$$\begin{aligned}
& X^2 \sin \theta_1 \sin \theta_2 + (Y^2 - Z^2) \cos \theta_1 \cos \theta_2 + XY' \sin 2\beta + 2\kappa_{oi} Z' \cos \theta_B \sin \beta - \kappa_{oi}^2 \\
& = \frac{1}{4} \kappa_{or}^2 \chi_h^{-2} (1 - 2q).
\end{aligned} \quad (2.47a)$$

$$\begin{aligned}
& Y' Z' \cos \theta_1 \cos \theta_2 + XZ' \sin \beta \cos \beta - \kappa_{oi} \cos \theta_B (X \cos \beta + Y' \sin \beta) \\
& = \frac{1}{4} \kappa_{or}^2 \chi_h^{-2} p \cos \delta.
\end{aligned} \quad (2.47b)$$

Since the quadratic equation (2.47) has two solutions, straight line ν and the dispersion surface generally intersect two times, and they called A_1 and A_2 as shown in Fig.2.3.

(v) Shape of dispersion surface

In SIA, the equation of the dispersion surface is represented as follows

$$\begin{aligned}
& X^2 \sin \theta_1 \sin \theta_2 + (Y^2 - Z^2) \cos \theta_1 \cos \theta_2 + XY' \sin 2\beta + 2\kappa_{oi} Z' \cos \theta_B \sin \beta - \kappa_{oi}^2 \\
& = \frac{1}{4} \kappa_{or}^2 |\chi_{hr}|^2 (1 - |k|^2), \quad \left(|k| \equiv \frac{|\chi_{hi}|}{|\chi_{hr}|} \right),
\end{aligned} \quad (2.48)$$

represents a hyperbola.



43

between -1 and 1. Therefore, the real part(Y') of (2.47a) exceeds the asymptotic line and the shape of the dispersion surface spreads more than the conventional dispersion surface, and the shape is expected to show a versatile variation.

(vi) Diagrammatic presentation of two-wave approximation

A convenient and important parameter named W exists in the conventional dynamical theory, and it is called *resonance error*. W of Fig. 2.3 expresses the deviation from diffraction conditions proportional to X . According to the definition of FK, W given by as follows

$$W = -\frac{X \sin 2\theta_B}{|\cos \theta_1 \cos \theta_2|^{1/2} \kappa_{0r} \bar{\chi}_h} \quad (2.49)$$

Here, W is compared with SIA. The resonance error in SIA is given by

$$W' = -\frac{X \sin 2\theta_B}{|\cos \theta_1 \cos \theta_2|^{1/2} \kappa_{0r} |\chi_{hr}|} \quad (2.50)$$

In case of $q=1$, $\bar{\chi}_h = |\chi_{hr}|$ because of $\chi_{hr}=0$. Therefore (2.49) of present theory is finite, but (2.50) will diverge. For this reason, in SIA, the physical examination cannot perform when $q=1$.

W will diverge in case of $\chi_{hr}=0$, and one cannot perform any physical examination. However, (2.49) of FK has none of singular point and that is no trouble on handling the equation. It is worth mentioning that Ishida *et al.*(1997) [8] used χ_{hr}^0 instead of χ_{hr} in (2.50) in order to avoid the divergence. The χ_{hr}^0 is shown in the following equation

$$\chi_{hr}^0 = -\frac{4\pi}{v\omega^2} \sum f_j^0 \exp(2\pi i \mathbf{h} \cdot \mathbf{r}_j) T_j \quad (2.51)$$

Since this χ_{hr}^0 does not become zero, resonance error by Eq(2.51) is no divergence in $q=1$. However, in the definition of Ishida, the formulae becomes complicated and the treatment is

inconvenient.

The meaning of W is examined in this paragraph. When reciprocal-lattice point H locate in the incidence plane and the glancing angle of the incident X-ray is α_0 , (2.49) is approximated as follows

$$W = (\alpha_0 - \alpha_{0L}) \sqrt{\frac{\cos \theta_1}{|\cos \theta_2|} \frac{\sin 2\theta_B}{n_0 \chi_h}} \quad (2.52)$$

Where α_{0L} is the glancing angle at $W=0$, n_0 is κ_0/K_0 in (2.25). W is proportional to the deviation $\alpha_0 - \alpha_{0L}$. Therefore W increases in the direction in which the glancing angle α_0 increases. In symmetrical reflection, (2.52) becomes the following [APPENDIX A]

$$W = \frac{\Delta \theta \sin 2\theta_B}{\chi_h} \quad (2.53)$$

Supposing $|W| \leq 4$, $\overline{\chi_h} \cong 2 \times 10^{-6}$, and the range of $\Delta \theta$ is about 2×10^{-5} deg ($= 4$ sec).

This paper assumes the following typical experiment system.

- (1) A polarization is adapted as σ -polarization. Hereafter $D_{o_{\parallel}}$ and $D_{h_{\perp}}$ will be expressed as D_o and D_h . In order to obtain the solution of π -polarization, the equation derived by σ -polarization can be used by multiplying both χ_{hr} and χ_h by $\cos 2\theta_B$.
- (2) Reciprocal-lattice point H is assumed to be in the incident plane (OHL plane in Fig.2.3). Generally, reciprocal-lattice point H not exists in the incident plane. In this case, however, W is modified as shown in [1].

2.2.3 Boundary Conditions

Assuming that a crystal is the parallel board of thickness H , as shown in Fig.2.4, there are two boundary conditions. In the first case, the diffracted and a transmitted waves goes into a crystal (Laue case, $\cos \theta_2 > 0$, Fig.2.4 (a)). In the other case, a diffracted wave comes out

from the surface of the crystal incident (Bragg case, $\cos \theta_2 < 0$, Fig 2.4 (b)).

A plane wave of $E_o \exp(-2 \pi i \mathbf{K}_o \cdot \mathbf{r})$ is injected from above upper the crystal as shown in Fig 2.4. A transmitted wave is connected to the incident wave at two tie points A_1 and A_2 as following two waves

$$D_o^{(1)}(\mathbf{r}) = D_o^{(1)} \exp(-2 \pi i \mathbf{k}_o^{(1)} \cdot \mathbf{r}), \quad (2.54a)$$

$$D_o^{(2)}(\mathbf{r}) = D_o^{(2)} \exp(-2 \pi i \mathbf{k}_o^{(2)} \cdot \mathbf{r}). \quad (2.54b)$$

These two transmitted waves in the crystal are connected to the transmitted vacuum wave $E_d \exp(-2 \pi i \mathbf{K}_d \cdot \mathbf{r})$ of the outside the exit surface the crystal ($z=H$). The diffracted wave in the crystal also connect to the following equations at two tie points

$$D_h^{(1)}(\mathbf{r}) = D_h^{(1)} \exp(-2 \pi i \mathbf{k}_h^{(1)} \cdot \mathbf{r}), \quad (2.55a)$$

$$D_h^{(2)}(\mathbf{r}) = D_h^{(2)} \exp(-2 \pi i \mathbf{k}_h^{(2)} \cdot \mathbf{r}). \quad (2.55b)$$

These diffracted waves connect to $E_h \exp(-2 \pi i \mathbf{K}_h \cdot \mathbf{r})$ which is the diffracted vacuum wave outside of the crystal, on the under surface of the crystal in the Laue case and on the upper surface of the crystal in the Bragg case.

The boundary conditions in the upper surface and the under surface of the crystal are shown in the following equation.

Laue case:

Upper surface ($z=0$):

$$D_o^{(1)} + D_o^{(2)} = E_o, \quad (2.56a)$$

$$D_h^{(1)} + D_h^{(2)} = 0. \quad (2.56b)$$

Under surface ($z=H$):

$$D_o^{(1)} \exp(-2 \pi i \mathbf{k}_{oz}^{(1)} H) + D_o^{(2)} \exp(-2 \pi i \mathbf{k}_{oz}^{(2)} H) = E_d \exp(-2 \pi i \mathbf{K}_d \cdot H), \quad (2.57a)$$

$$D_h^{(1)} \exp(-2 \pi i k_{hz}^{(1)} H) + D_h^{(2)} \exp(-2 \pi i k_{hz}^{(2)} H) = E_h \exp(-2 \pi i K_{hz} H). \quad (2.57b)$$

Bragg case:

Upper surface ($z=0$):

$$D_o^{(1)} + D_o^{(2)} = E_o, \quad (2.58a)$$

$$D_h^{(1)} + D_h^{(2)} = E_h. \quad (2.58b)$$

Under surface ($z=H$):

$$D_o^{(1)} \exp(-2 \pi i k_{oz}^{(1)} H) + D_o^{(2)} \exp(-2 \pi i k_{oz}^{(2)} H) = E_d \exp(-2 \pi i K_{dz} H), \quad (2.59a)$$

$$D_h^{(1)} \exp(-2 \pi i k_{hz}^{(1)} H) + D_h^{(2)} \exp(-2 \pi i k_{hz}^{(2)} H) = 0. \quad (2.59b)$$

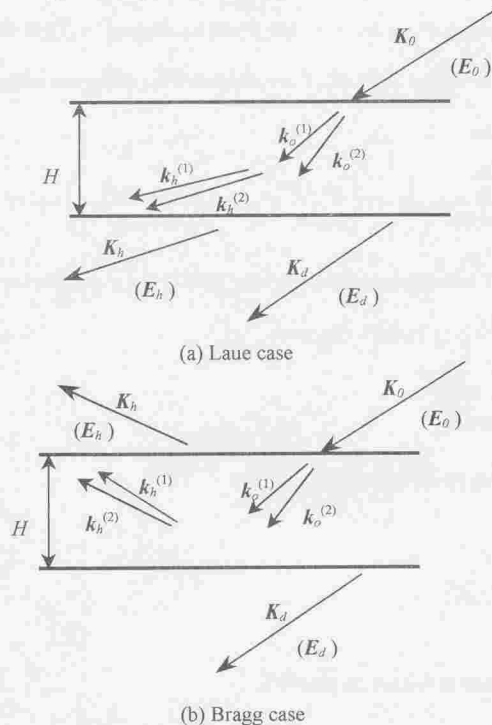


Fig 2.4 Diffraction conditions.

Here, k_{oz} , k_{hz} , K_{dz} and K_{hz} are the components perpendicular to the crystal surface of k_o , k_h , K_d and K_h .

2.2.4. Diffraction Intensity

(i) Introductory

Using j as the number of tie point, the relationship between D_o and D_h for every tie points is given by

$$D_h^{(j)} = R^{(j)} D_o^{(j)} \quad (2.60)$$

When diffraction conditions are decided $\Delta\theta$, W will be obtained by (2.53), and X is decided by (2.49) using the W . Based on (2.46), Y coordinates of the dispersion surface is shown by the following equation

$$Y = \frac{\kappa_{or} \overline{\chi_h}}{2|\cos\theta_1 \cos\theta_2|^{1/2}} \left\{ (-1)^c \left[\frac{\sin 2\beta}{\sin 2\theta_B} W + ig \frac{\cos\theta_B \sin\beta}{|\cos\theta_1 \cos\theta_2|^{1/2}} \right] + (-1)^j \sqrt{Q} \right\} \quad (2.61)$$

In the equation, $c=1$ is Bragg case and $c=2$, Laue case. Q and g' are given by

$$Q = (W + ig')^2 + (-1)^c (1 - 2q + i2p \cos\delta), \quad (2.62)$$

$$g' = g \frac{\sin\theta_B \cos\beta}{|\cos\theta_1 \cos\theta_2|^{1/2}} \quad (2.63)$$

g and g_o will be shown by the following equations

$$g = g_o \sqrt{q}, \quad (2.64)$$

$$g_o = \frac{\chi_{0i}}{|\chi_{hi}|} \quad (2.65)$$

g_o will be examined as follows. In generally,

$$|\chi_{0i}| \geq |\chi_{hi}| \quad (2.66)$$

$|g_0| \geq 1$ will result. As shown by (2.30 b), since χ_{0i} is always negative, g_0 is also negative. The correction term T_j for temperature in (2.17) is 1 at maximum, and is smaller than 1 for the limited temperature. Therefore, assuming

$$|\chi_{0i}| = |\chi_{0i(T_j=1)}|, \quad (2.67)$$

When T_j is one or less, $|g_0|$ is larger than 1. Generally, if temperature rises, since T_j becomes small, $|g_0|$ becomes larger than 1.

ξ_o is calculated by substituting Y of (2.61) and X of (2.49) to (2.45), and is given by

$$\xi_o = \frac{\kappa_{or} \overline{\chi_h}}{2} \sqrt{\frac{\cos \theta_1}{|\cos \theta_2|}} \left\{ (-1)^e \left[W + ig' \frac{\cos \theta_B \sin \beta}{|\cos \theta_1 \cos \theta_2|^{1/2}} \right] + (-1)^f \sqrt{Q} \right\}. \quad (2.68)$$

substituting ξ_o to $|k_o| - \kappa_o = \xi_o - \kappa_{0i}$, is given by

$$|k_o| - \kappa_o = \frac{\kappa_{or} \overline{\chi_h}}{2} \sqrt{\frac{\cos \theta_1}{|\cos \theta_2|}} \left[(-1)^e (W + ig') + (-1)^f \sqrt{Q} \right]. \quad (2.69)$$

substituting (2.69) to (2.60) and $R^{(j)}$ is obtained by the following equation

$$R^{(j)} = \frac{\overline{\chi_h}}{\chi_h} \sqrt{\frac{\cos \theta_1}{|\cos \theta_2|}} \cdot \left[(-1)^e (W + ig') + (-1)^f \sqrt{Q} \right]. \quad (2.70)$$

Since $R^{(j)}$ was obtained from the above consideration, and $D_0^{(j)}$ is derived as following.

(Laue case)

As shown in the following equation, $D_0^{(j)}$ is obtained from the boundary conditions of (2.56 b) and (2.60)

$$D_o^{(2)} = \frac{D_h^{(2)}}{R^{(2)}} = -\frac{D_h^{(1)}}{R^{(2)}}. \quad (2.71)$$

Therefore, $D_o^{(1)}$ and $D_o^{(2)}$ are given by the following equation from (2.56 a)

$$D_o^{(1)} = -\frac{R^{(2)}}{R^{(1)} - R^{(2)}} E_0, \quad (2.72a)$$

$$D_o^{(2)} = \frac{R^{(1)}}{R^{(1)} - R^{(2)}} E_0. \quad (2.72b)$$

Substituting $R^{(j)}$ of (2.70) to (2.72), (2.73) is obtained as $D_o^{(j)}$ of Laue case

$$D_o^{(j)} = (-1)^j \frac{-(W + ig' + (-1)^{j-1} \sqrt{Q})}{2\sqrt{Q}} E_0. \quad (2.73)$$

(Bragg case)

Boundary conditions (2.59b) are as follows

$$D_h^{(1)} = -R^{(2)} D_o^{(2)} \exp[-2\pi i H(k_{hz}^{(2)} - k_{hz}^{(1)})], \quad (2.74a)$$

$$D_h^{(2)} = -R^{(1)} D_o^{(1)} \exp[2\pi i H(k_{hz}^{(2)} - k_{hz}^{(1)})]. \quad (2.74b)$$

(2.58 a) is modified as follows

$$\begin{aligned} D_o^{(1)} + D_o^{(2)} &= D_o^{(1)} + \frac{D_h^{(2)}}{R^{(2)}} \\ &= D_o^{(1)} - \frac{R^{(1)}}{R^{(2)}} D_o^{(1)} \exp[2\pi i H(k_{hz}^{(2)} - k_{hz}^{(1)})] = E_0. \end{aligned} \quad (2.75)$$

$D_o^{(1)}$ is obtained equation using (2.74) and (2.75) as follow

$$D_o^{(1)} = \frac{R^{(2)}}{R^{(2)} - R^{(1)} \exp[2\pi i H(k_{hz}^{(2)} - k_{hz}^{(1)})]} E_0, \quad (2.76a)$$

By the same method, as $D_o^{(2)}$

$$D_o^{(2)} = \frac{R^{(1)}}{R^{(1)} - R^{(2)} \exp[-2\pi i H(k_{hz}^{(2)} - k_{hz}^{(1)})]} E_0. \quad (2.76b)$$

Since $k_{hz}^{(2)} - k_{hz}^{(1)}$ is the difference of tie points on Y coordinates in reciprocal-lattice space as shown in Fig. 2.3, the following relationship is establish

$$k_{hz}^{(2)} - k_{hz}^{(1)} = Y^{(2)} - Y^{(1)}. \quad (2.77)$$

Using (2.61), the relationship of (2.77) will become to following

$$Y^{(2)} - Y^{(1)} = \frac{s}{\pi} \sqrt{Q}. \quad (2.78)$$

In this paragraph, the meaning of s discussed. The present s is defined by

$$s = \frac{\pi \kappa_{or} \chi_h}{|\cos \theta_1 \cos \theta_2|^{1/2}}. \quad (2.79a)$$

s is shown by the following equation using $|\chi_{hr}|$ in SIA

$$s' = \frac{\pi \kappa_{or} |\chi_{hr}|}{|\cos \theta_1 \cos \theta_2|^{1/2}}. \quad (2.79b)$$

For this reason, when $q=1$, since χ_{hr} is zero, s' is also zero. In $s'=0$, it become to 0 that the difference between two tie points shown by (2.78). However, s of this paper does not become zero in $q=1$, two solution with the hyperbola in the dispersion surface inconsistent with result by SIA.

Substituting (2.61) and (2.77) to (2.76), and $D_o^{(j)}$ of Bragg case is given by

$$D_o^{(j)} = (-1)^j \frac{(W + ig' + (-1)^j \sqrt{Q}) \exp((-1)^j isH \sqrt{Q})}{(W + ig' + \sqrt{Q}) \exp(isH \sqrt{Q}) - (W + ig' - \sqrt{Q}) \exp(-isH \sqrt{Q})} E_o. \quad (2.80)$$

In an experiment, the X-ray of the limited cross section incidents into the crystal as shown in Fig 2.5. Generally, the cross section of the diffracted wave differs from the cross section of the incident X-ray. Therefore, let P_o is the energy per unit time of the incident X-ray, P_d one of the transmitted wave, and P_h one of the diffracted wave, the following relationship is obtained also in consideration of Bragg case ($\cos \theta_2 < 0$)

$$\frac{P_h}{P_o} = \left| \frac{E_h}{E_o} \right|^2 \frac{|\cos \theta_2|}{\cos \theta_1}, \quad (2.81a)$$

$$\frac{P_d}{P_o} = \left| \frac{E_d}{E_o} \right|^2. \quad (2.81b)$$

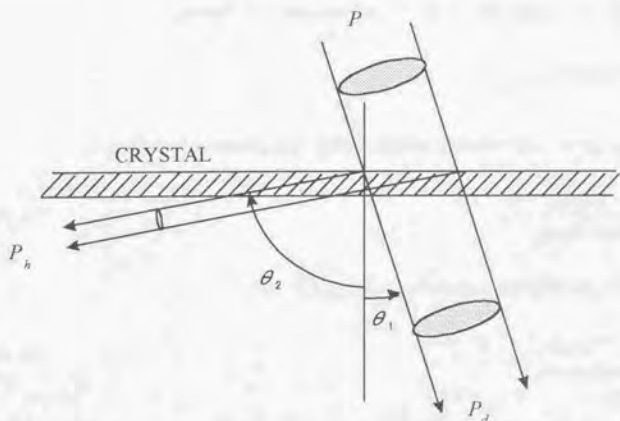


Fig 2.5. Experimental conditions

(ii) **Diffracted intensity and transmitted intensity**

E_h / E_o and E_d / E_o are obtained from the boundary conditions of (2.56), (2.57), (2.58), and (2.59). The diffracted and the transmitted intensities of the Laue case and Bragg case in the crystal of the finite thickness are obtained from using relation of (2.60), (2.73), (2.76), (2.80), and (2.81).

Laue case:

$$\frac{P_h}{P_0} = (1 - 2p \sin \delta) \exp(-\mu_0 H') \left| \frac{\exp(isH\sqrt{Q}) - \exp(-isH\sqrt{Q})}{2\sqrt{Q}} \right|^2, \quad (2.82a)$$

$$\frac{P_d}{P_0} = \exp(-\mu_0 H') \left| \frac{(W + ig^+ + \sqrt{Q}) \exp(isH\sqrt{Q}) - (W + ig^- - \sqrt{Q}) \exp(-isH\sqrt{Q})}{2\sqrt{Q}} \right|^2, \quad (2.82b)$$

Bragg case: (see[9])

$$\frac{P_b}{P_0} = (1 - 2p \sin \delta) \left| \frac{\exp(isH\sqrt{Q}) - \exp(-isH\sqrt{Q})}{(W + ig' + \sqrt{Q}) \exp(isH\sqrt{Q}) - (W + ig' - \sqrt{Q}) \exp(-isH\sqrt{Q})} \right|^2 \quad (2.83a)$$

$$\frac{P_d}{P_0} = \exp(-\mu_0 H') \left| \frac{2\sqrt{Q}}{(W + ig' + \sqrt{Q}) \exp(isH\sqrt{Q}) - (W + ig' - \sqrt{Q}) \exp(-isH\sqrt{Q})} \right|^2 \quad (2.83b)$$

Here, H' is defined as follows

$$H' = \frac{\cos \theta_B \sin \beta}{\cos \theta_1 \cos \theta_2} H = \frac{1}{2} \left(\frac{1}{\cos \theta_1} + \frac{1}{\cos \theta_2} \right) H \quad (2.84)$$

H is mean distance along which the diffracted and the transmitted waves pass within the crystal in Laue case, and is positive. In Bragg case, however, it is an average of the difference of the distance along which the diffracted and the transmitted waves pass within the crystal and is negative.

The symmetrical factor a is defined by the following equation using θ_1 and θ_2 of the dispersion surface in Fig. 2.3

$$a = \frac{\cos \theta_1}{|\cos \theta_2|} \quad (2.85)$$

Using this a , g' of (2.63) is expressed as follows

$$g' = g \frac{a-1}{2\sqrt{a}}, \quad (\text{Laue case}) \quad (2.86a)$$

$$g' = g \frac{a+1}{2\sqrt{a}} \quad (\text{Bragg case}) \quad (2.86b)$$

General formulae that obtains the diffracted and the transmitted intensities in (2.82) and (2.83) has the following characteristics.

- (1) Each expression has term $\exp(-isH\sqrt{Q})$ expressing the wave from the tie point 1 and term $\exp(+isH\sqrt{Q})$ expressing the wave from the tie point 2.

(2) $(1 - 2p \sin \delta)$ in the diffracted intensity provides the polarity information in the crystal by phase difference δ between χ_{hr} and χ_{hu} .

(3) The denominator and the numerator of the transmitted-intensity expressions are reversed in Laue case and Bragg case.

(4) The diffracted and the transmitted intensities of Laue case, and the transmitted intensity in Bragg case are depend on the mean absorption μ_0 .

(iii) Integrated reflecting power

In this section, the integrated reflecting power by this paper is examined comparing with the result of SIA. In order to measure the intensity curve (rocking curve) of (2.82), incident X-rays are required very parallel. In the usual source of X-rays, however, the intensity obtained by the generator is weak, and the parallelism are poor. Therefore, in conventionally, the integrated reflecting power is measured instead of the rocking curve. Integrated reflection intensities is obtained by multiplying the intensity of incident X-rays to the integrated reflecting power.

According to FK [10], the integrated reflecting power R_h of the diffracted wave by the angle-dispersive method is expressed as follows

$$\left\{ \begin{array}{l} R_h = \left(\frac{|\cos \theta_z|}{\cos \theta_1} \right)^{1/2} \frac{\overline{\chi_h}}{\sin 2\theta_B} R_h^w \\ R_h^w = \int \frac{P_h}{P_o} dW \end{array} \right. \quad (2.87)$$

In many conventional textbooks, $|\chi_{hr}|$ has been used instead of $\overline{\chi_h}$ in (2.87). The energy-dependability of the integrated reflecting power in that case is satisfactory when surveying in

a wide range. However, R_h is zero when $|\chi_{hr}|=0$. For this reason, the precise argument needs (2.87).

2.2.5 Energy Flow

Laue(1952)[11] pointed out that the diffracted and the transmitted waves belonging to one tie point in a crystal without being able to exist independently. However they are united and are transmitted. The energy flow of the electromagnetic field is expressed by a Poynting vector. The Poynting vector of two-wave approximations is expressed by the following equation in [APPENDIX B] when calculated by applying the FK method, referring of Miyake [1]

$$\overline{\overline{S}} = \frac{c}{8\pi} \exp[4\pi(k_o \cdot r)] \left[\frac{k_o}{|k_o|} |D_o|^2 + \frac{k_h}{|k_h|} |D_h|^2 \right]. \quad (2.88)$$

The term of exp shows an attenuation by absorption and $|D_o|$ and $|D_h|$ are the amplitudes of the electric displacement of the diffraction and the transmitted waves. $\overline{\overline{S}}$ expresses a time-wise and space-wise averages of the Poynting vector, and is decided by the dispersion surface and the boundary conditions.

2.2.6 Wave Field in Crystal

The general expression of the pendellösung beat and the standing wave in the crystal are derived below:

(i) Pendellösung beat

As mentioned earlier, the pendellösung beat appears in $I(r)$ which is the sum of waves from the tie points 1 and 2 in the crystal

$$I_h(r) = |D_h^{(1)}(r) + D_h^{(2)}(r)|^2, \quad (2.89a)$$

$$I_o(r) = |D_o^{(1)}(r) + D_o^{(2)}(r)|^2. \quad (2.89b)$$

As for Laue case, the following equations are obtained from (2.89)

$$I_h(z) = (1 - 2p \sin \delta) \exp(-\mu_0 z') \frac{\cos \theta_1}{\cos \theta_2} \left| \frac{\exp(isz\sqrt{Q}) - \exp(-isz\sqrt{Q})}{2\sqrt{Q}} E_0 \right|^2, \quad (2.90a)$$

$$I_o(z) = \exp(-\mu_0 z') \left| \frac{(W + ig' + \sqrt{Q}) \exp(isz\sqrt{Q}) - (W + ig' - \sqrt{Q}) \exp(-isz\sqrt{Q})}{2\sqrt{Q}} E_0 \right|^2. \quad (2.90b)$$

As for Bragg case, the following equations are obtained from (2.89)

$$I_h(z) = (1 - 2p \sin \delta) \frac{\cos \theta_1}{|\cos \theta_2|} \left| \frac{\exp(isz\sqrt{Q}) - \exp(-isz\sqrt{Q})}{(W + ig' + \sqrt{Q}) \exp(isz\sqrt{Q}) - (W + ig' - \sqrt{Q}) \exp(-isz\sqrt{Q})} E_0 \right|^2, \quad (2.91a)$$

$$I_o(z) = \exp(-\mu_0 z') \left| \frac{2\sqrt{Q}}{(W + ig' + \sqrt{Q}) \exp(isz\sqrt{Q}) - (W + ig' - \sqrt{Q}) \exp(-isz\sqrt{Q})} E_0 \right|^2. \quad (2.91b)$$

Where, z is the downward depth perpendicularly from the surface of the crystal (see Fig. 2.3).

(ii) Standing wave in a crystal

The standing wave in the crystal is the sum of the wave in the same tie point, and is shown in the following equation (2.92)

$$\begin{aligned} I^{(j)}(r) &= |D_o^{(j)} \exp(-2\pi i k_o^{(j)} \cdot r) + D_h^{(j)} \exp(-2\pi i k_h^{(j)} \cdot r)|^2 \\ &= |D_o^{(j)}|^2 \exp(4\pi k_{oz}^{(j)} z) [1 + |R^{(j)}|^2 + 2|R^{(j)}| \cos(2\pi h \cdot r - \Omega^{(j)})], \quad (2.92) \end{aligned}$$

$$R^{(j)} = |R^{(j)}| \exp(i\Omega^{(j)}). \quad (2.93)$$

Where, $\Omega^{(j)}$ is the phase angle of (2.93). The standing wave is shown in [] on the right-hand side of (2.92) as described later.

2.3 Diffracted Wave and Transmitted Wave in Laue case

In the following, using the fundamental equations obtained by section 2.2, a diffracted intensity, transmitted intensity, dispersion surface, Poynting vector and the wave field in a crystal in Laue case are examined by the variation of q (ratio of $|\chi_{hr}|$ and $|\chi_{ht}|$), H (crystal thickness), and δ (phase difference between χ_{hr} and χ_{ht}).

2.3.1. Rocking Curve

The characteristic of the dynamical diffraction appears as the change of the intensity near the Bragg condition, forever rocking curves around the zero are investigated by variable W . The conditions of the following discussion have symmetrical reflection.

(i) Dependence on q

The range of q is 0 to 1. $\chi_h \chi_{-h}$ of (2.44) is the real number of positive for $q=0$, it is the real number of minus for $q=1$, and it is the pure imaginary number for $q=0.5$. Rocking curves are examined in these three cases. The diffracted intensity at $W=0$ becomes zero when $q=0$ and $sH=\pi$, the crystal thickness is chosen with this condition.

a) In case of $q=0$

The condition exist two cases for $q=0$, and one does not have absorption ($\chi_{0i}=0$) and

another has absorption ($\chi_{hi} = 0$). In $q = 0$, if there is no absorption, $\chi_{oi} = \chi_{hi} = 0$ are satisfied. When $\chi_{hi} = 0$ and there is the absorption, χ_{oi} is not zero. As the actual crystal, the absorption is not zero completely. For this reason, we examine the dynamical diffraction when the absorption cannot be neglected, and when there is no absorption. The dynamical diffraction with the absorption at $q=0$ had been examined in the conventionally theory.

When there is absorption for $q=0$, (2.82) becomes following equations

$$\frac{P_h}{P_o} = \exp(-\mu_0 H') \frac{\sin^2(sH\sqrt{W^2+1})}{W^2+1}, \quad (2.94a)$$

$$\frac{P_d}{P_o} = \exp(-\mu_0 H') \frac{W^2 + \cos^2(sH\sqrt{W^2+1})}{W^2+1}, \quad (2.94b)$$

Rocking curves of diffracted and transmitted waves in $sH=\pi$ by (2.94), are shown in Fig 2.6 by the dotted lines. In this paper, $g=-0.1$ ($\mu_0 H' = -0.2\pi$) is selected. When χ_{hi} becomes zero near Ga K-absorption edge of GaAs 200 reflection, g can be estimated to be about $g=-0.1$, by calculation using the PH method (the problem is examined by Chapter III in detail). When the mean absorption is negligible in (2.94), the exp term is set to 1. Equations (2.94) becomes the same as that of (3.142) of Zachariasen [12] which neglected absorption. Therefore, When $\chi_{oi} \neq 0$, (2.94) can be interpreted the equation that the exp term is added to the formula at $\chi_{oi} = 0$.

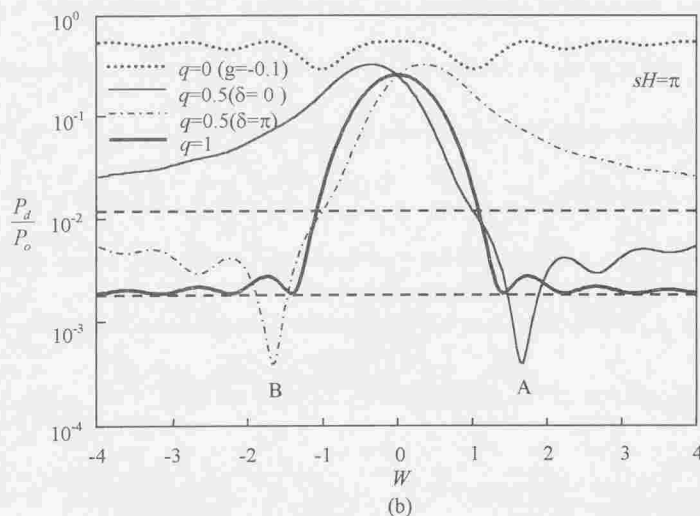
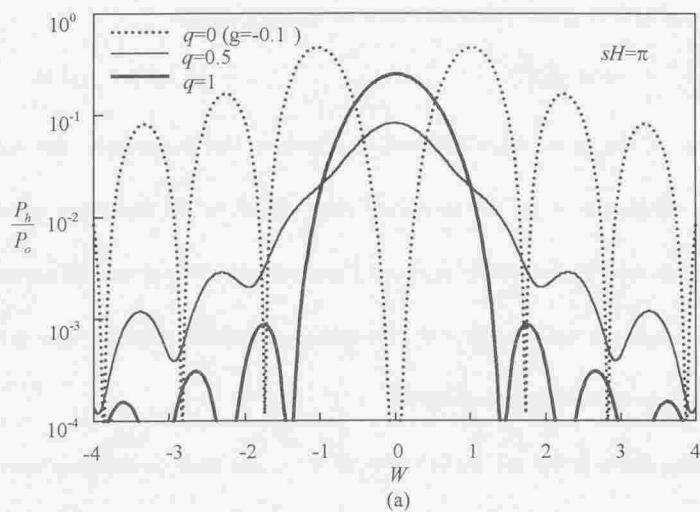


Fig.2.6 The rocking curves in the symmetric Laue case for $q = 0.0, 0.5$ and 1.0 when $sH = \pi$ and $g_0 = -1$ ($g = -0.1$). (a) Diffracted waves. (b) Transmitted waves.

The sum of (2.94a) and (2.94b) is shown in the following equation

$$\frac{P_b}{P_0} + \frac{P_d}{P_0} = \exp(-\mu_0 H'). \quad (2.95)$$

(2.95) shows that the amount of incident X-rays remaining after absorption is distributed to the diffracted wave and the transmitted wave. Therefore, the transmitted intensity decreases as the diffracted intensity increased. Conversely, the diffracted intensity decreases as the transmitted intensity increased. For this reason, even when there is absorption, (2.94) does not show the anomalous transmission.

Rocking curves in Fig. 2.6 are symmetry to $W=0$, and clear pendellösung beats is presented. The period of pendellösung beat is π in $|W| > 1$. This is understood from the square term of sin and cos functions in (2.94). The dependability will the crystal thickness of this pendellösung beat is examined in after subparagraph (2.3.5.ii)

b) In case of $q=1$

In case of $q=1$, $\chi_{hr}=0$ and $\chi_{0h} \neq 0$ will result in case of $\chi_{hu} \neq 0$. Therefore, there is not two cases for χ_{0h} as $q=0$. In this case, following equations are obtained from (2.82) as $g_0=-1$

$$\frac{P_b}{P_0} = \exp(-\mu_0 H') \left| \frac{\exp(isH\sqrt{W^2-1}) - \exp(-isH\sqrt{W^2-1})}{2\sqrt{W^2-1}} \right|^2, \quad (2.96a)$$

$$\frac{P_d}{P_0} = \exp(-\mu_0 H') \left| \frac{(W + \sqrt{W^2-1}) \exp(isH\sqrt{W^2-1}) - (W - \sqrt{W^2-1}) \exp(-isH\sqrt{W^2-1})}{2\sqrt{W^2-1}} \right|^2. \quad (2.96b)$$

Rocking curves obtained by (2.96) are shown in Fig.2.6 as the thick solid lines. Unlike the case of $q=0$, both diffracted-intensity (a) and transmitted-intensity (b) shape the peak at $W=$

0. The ratios of the diffracted and the transmitted intensities to the incident intensity are both about 0.25 at $W=0$. This effect of the making peak at $W=0$ is the Borrmann effect. The ups and downs in the tail of the rocking curves are the pendellösung beat, and the period is π in $|W| > 1$. These pendellösung beats are made dents and bumps on the intensity obtained by the mean absorption (dashed line) in transmitted intensity. Rocking curves of the diffracted and the transmitted intensities are symmetry to $W=0$.

The quantity of the anomalous transmission at $W=0$ is calculated. (2.96) will become following equations when $q=0$ and $W=0$

$$\frac{P_h}{P_o} = \frac{1}{4} [1 - 2 \exp(2gsH) + \exp(4gsH)], \quad (2.97a)$$

$$\frac{P_d}{P_o} = \frac{1}{4} [1 + 2 \exp(2gsH) + \exp(4gsH)]. \quad (2.97b)$$

Fig.2.7 shows the influence of sH in (2.97) when $g_0=-1$. If sH increases, the diffracted-intensity (dashed line) approaches from 0 to 0.25, and the transmitted-intensity (solid line) will approach from 1 to 0.25. This phenomenon is clear also from (2.97). Therefore, if sH is more than 6 and the crystal is sufficiently thick, 25% of both diffracted-intensity and transmitted-intensity is both penetrated anomaly regardless of the crystal thickness. These intensities are obtained by the anomalous transmission. That is, if the crystal is sufficiently thick at $W=0$, the half of the incident X-ray is absorbed by the crystal and the other half penetrate it.

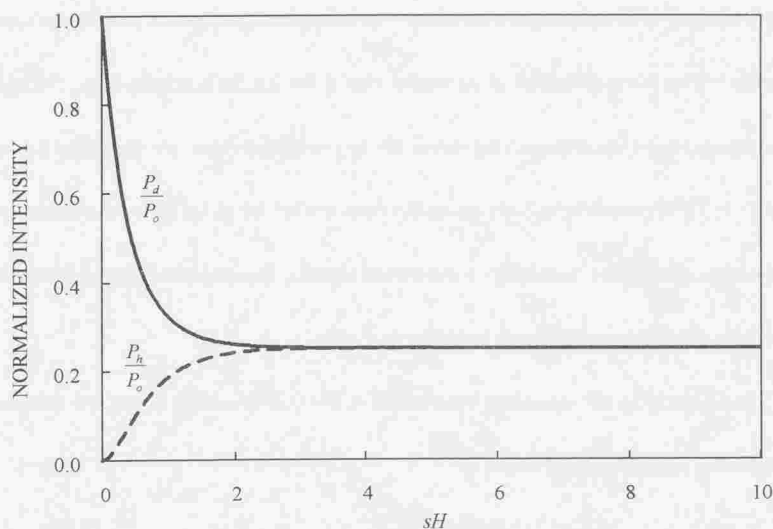


Fig 2.7 The change of the intensity with crystal thickness in the symmetric Laue case for $W=0$ when $q=1$ and $g_o=-1.0$.

c) In case of $q=0.5$

Following, rocking curves at $|\chi_{hr}|=|\chi_h|$ ($q=0.5$) are examined. Rocking curves of the diffracted intensity are shown in Fig.2.6 (a) as the thin solid line. Rocking curves of the transmitted intensity are shown in Fig.2.6 (b). Here, the thin solid line is $\delta=0$ and the dot dashed line is $\delta=\pi$. The rocking curve of the diffracted intensity has a peak at $W=0$, and it is symmetry to $W=0$. Rocking curves of the transmitted intensity are asymmetry to $W=0$. The peak shift for $\delta=0$ is the negative side slightly from $W=0$, and one of $\delta=\pi$ is the positive side slightly. In case of $\delta=0$, the transmitted intensity in the negative region of W is larger

than the intensity of the mean absorption (dashed line), and in the positive region is smaller than the mean absorption. The asymmetry is reversed in $\delta = \pi$. The asymmetry of the rocking curve by δ is also examined in the dispersion surface of the paragraph (2.3.3). In case of $\delta = 0$, the part of the intensity (Point A in Fig. 2.6(b)) in the positive region of W becomes weak remarkably. In the case of $\delta = \pi$, the portion is in the negative region (Point B). This effect is called nontransparent effect in this paper. This effect will be examined in detail later.

Pendellösung beats appear over rocking curves of diffracted-intensity (a) and transmitted-intensity (b) even though both beats are weak. The pendellösung beat of the diffracted intensity weakly vibrates from $W = 0$ to the tail. In case of $q = 0$ or $q = 1$, the rocking curves exist portion that diffracted intensities becomes zero. However it doesn't exist for $q = 0.5$. This effect will be discussed later in paragraph (2.3.3).

(ii) Dependence on crystal thickness H

In (2.82), sH including thickness is used as a parameter to examine the crystal thickness. Assuming that s is constant, since sH is proportional to the crystal thickness H , sH is chosen. As in (i), three cases are considered for q , namely, $q = 0, 0.5$ and 1 . Fig. 2.8 shows the results of calculations made by varying sH to $\pi/2, \pi$ and $3\pi/2$ for each of q in (2.82).

a) In case of $q = 0$ ($g = -0.1$)

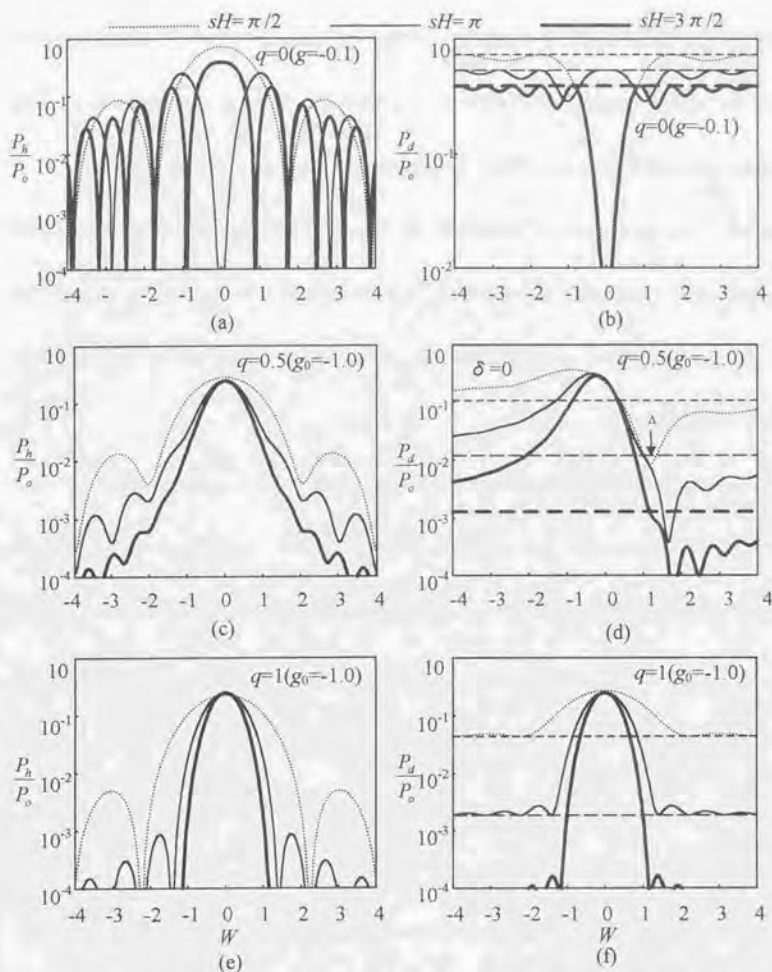


Fig.2.8 The rocking curves of diffracted and transmitted waves in the symmetric Laue case for $sH=\pi/2, \pi, 3\pi/2$ when $\delta=0$. (a)(b) $q=0$ and $g_0=-0.1$, (c)(d) $q=0.5$ and $g_0=-1$, (e)(f) $q=1$ and $g_0=-1$

When sH increases with $\pi/2, \pi$ and $3\pi/2$ in Fig.2.8, the diffracted intensity (a) is affected by absorption and the wave heights of pendellösung beats become small. Transmitted

intensity (b) weakens as the whole affected by mean absorption (dashed lines) proportionate to increasing thickness. As shown in (2.95), the sum of diffracted intensities and transmitted intensities is the quantity remaining affected by the mean absorption and is constant. The sum shows fixed value. In this case, however, the effect of the anomalous transmission does not appear even though the crystal thickness becomes thick. In $|W| > 1$, the period of the pendellösung beat shortens to 1/2 and 1/3 when the crystal thickness becomes twice and 3 times. Changing of the period of the pendellösung beat is in agreement with the result of the conventional dynamical theory without absorption.

b) *In case of $q = 0.5$ ($g_0 = -1$)*

In this case, when crystal thickness increases, diffracted-intensity (c) will become weak quickly in the tail of the rocking curve. However, the intensity at $W = 0$ does not weaken and rocking curves shapes the peak by Borrmann effect, approaching the peak value of 0.25. When the crystal thickness increases, the transmitted-intensity (d) in $|W| > 1$ will decrease quickly as in diffracted intensities. However, the peak near $W = 0$ does not decrease. The transmitted rocking curve is asymmetry to $W = 0$, and has the peak in the negative side of W when $\delta = 0$. The peak is in the positive side of W when $\delta = \pi$. Since the shape of rocking curves when $\delta = \pi$ is reversed one of $\delta = 0$, Fig. 2.8 showed only $\delta = 0$. When sH increases, the peak of the rocking curve of the transmitted intensity becomes sharp gradually and the intensity approaches the constant value of 0.25 as in diffracted intensities at $W = 0$.

The period of the pendellösung beat by the increase in thickness changes as in $q=0$. However, the peak height of pendellösung beats is different from that when $q=0$. Rocking-curves of the diffracted intensity(c) has the peak at $W=0$, and is symmetry. The intensity of the tail becomes weak remarkably as the crystal becomes thick. The pendellösung beat of transmitted intensity (d) is not clearly visible in the negative side of W . However, it is clear on the positive side. Since it is large that the difference of the amplitude of waves from tie points 1 and 2 when $q=0.5$, the amplitude of the pendellösung beat becomes smaller than $q=0$. This will be discussed further in the paragraph for dispersion surface in detail.

In Fig 2.8(d), there is the point A which the transmitted intensity becomes weak remarkably on the positive side of W . Increase of sH moves the point A in the direction in which $|W|$ increases, and the depth becomes deep gradually. In the point A, X-rays do not penetrate completely in specific sH . The nontransparent effect to X-rays shown in Fig 2.6(b) and 2.8(d) was discovered by the authors et al.(1994) [13] and is examined further in paragraph 2.3.2.

c) In case of $q=1$ ($g_0=-1$)

Fig.2.8(e) and (f) show change of the rocking curve when crystal thickness gradually increase. The tail of rocking curves in diffracted intensity(e) and transmitted intensity (f) become small rapidly, when the crystal thickness increases. By Borrmann effect, the peak of rocking curves becomes sharp notably as the crystal thickness increases, and the intensity at

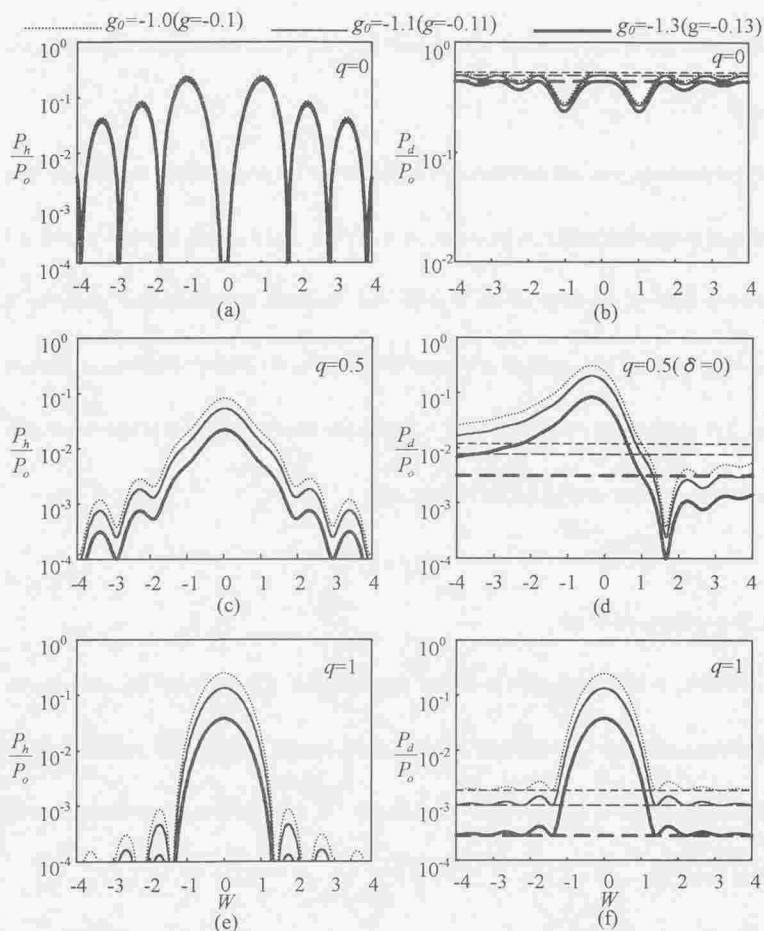


Fig.2.9 The rocking curves of diffracted and transmitted waves in the symmetric Laue case for several $g_0(g)$ when $sH = \pi$, $\delta = 0$. (a)(b) $q=0$; (c)(d) $q=0.5$; (e)(f) $q=1$.

$W=0$ approaches 0.25. If the monochromator can develop using the anomalous transmission in $q=1$, the dispersion angle will be narrow about 1 sec. The anomalous transmission by this

Borrmann effect will be examined later in detail from dispersion surfaces and wave fields in a crystal.

A pendellösung beat will become small remarkably, if the crystal thickness increases. The period of the pendellösung beat by the increase in the crystal thickness changes as $q=0$ and $q=0.5$ in $|W| > 1$. Rocking curves of diffracted intensities and transmitted intensities is symmetry to $W=0$. The minimum of the pendellösung beat for diffracted intensities becomes zero. The minimum of the pendellösung beat of transmitted intensities is in agreement with the intensity (dashed line) by the mean absorption.

(iii) Dependence on $g(g_0)$

As defined in (2.65), $g(g_0)$ is in inverse proportion to χ_{hi} which will become small as temperature increases as shown by (2.20b). For this reason, $|g(g_0)|$ will become large as temperature increases. In symmetrical reflection, if $K_0 = \kappa_{or}$ is approximated, $\mu_0 H$ is as follow from (2.31)

$$\mu_0 H = -2gsH \cos \theta_B. \quad (2.98)$$

In (2.98), if the crystal temperature rises, $|g(g_0)|$ will become large. As the result, the mean absorption μ_0 also becomes large. Fig.2.9 shows rocking curves of diffracted intensity (a, c, e) and the transmitted intensity (b, d, f) is changed for $q=0, 0.5$, and 1 assuming $sH=\pi$.

Even when g_0 is not calculated in $q=0$, g is directly obtained from (2.64). In the same

viewpoint as (ii), rocking curves of diffracted intensity (a) and transmitted intensity (b) are examined by change g to -0.1, -0.11, and -0.13. Intensities of rocking curves becomes weaker slightly uniformly to increase of g .

In $q = 0.5$ and $q = 1$, rocking curves shown in Fig.2.9 (c), (d), (e) and (f) when $|g_0|$ increases with 1.0, 1.1 and 1.3. Here, if $|g_0|$ becomes large, diffracted intensities and a transmitted intensities will become small uniformly like $q = 0$. This effect is understood from the fact that $g(g_0)$ dependence only $\exp(-\mu_0 H')$.

(iv) Dependence on phase difference δ

Since the imaginary part of Q in (2.62) is zero when q is 0 and 1, the dependence on δ appears in $0 < q < 1$. When the crystal has the center of symmetry, χ_{hr} and χ_{hi} can express both the real number and the Friedel's law is satisfied. In this case, the value of δ is either 0 or π . Although the rocking curve was symmetry to $W = 0$ when $q = 0$ and $q = 1$, the other rocking curve was asymmetry. In the further, dependence on δ of rocking curves is examined to $q = 0.5$ which is the middle of $q = 0$ and $q = 1$.

Fig.2.10 shows rocking curves in case of $\delta = 0$ and $\delta = \pi$ when $q = 0.5$ and $sH = \pi/2$. The diffracted intensity is shown by the thin solid line and the transmitted intensity is shown by the thick solid line and the thick dashed line. Although the rocking curve of the diffracted intensity is symmetry to $W = 0$, the rocking curve of a transmitted intensity is asymmetry. Since the rocking curve of the transmitted intensity of $\delta = 0$ (thick solid line) and that of $\delta = \pi$ (thick dashed line) is mirror symmetry to $W = 0$, namely, $I(0, W)$ is equal to $I(\pi, -W)$.

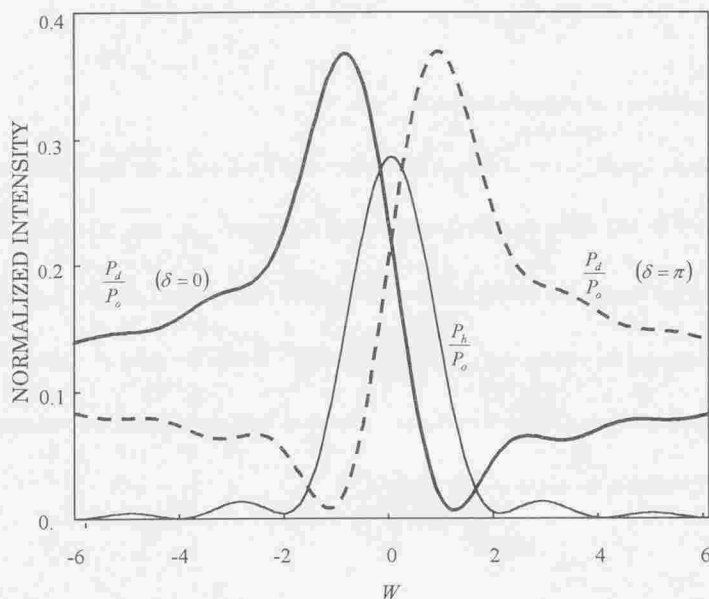


Fig.2.10 The calculated rocking curves in the symmetric Laue case for $q=0.5$, $g_0=-1$ and $sH = \pi/2$. The thin solid line is the curve of the diffracted wave. The thick solid and dashed lines are the curves of the transmitted wave for $\delta=0$ and $\delta = \pi$, respectively.

The asymmetry of rocking curves in transmitted intensities appears to the shift of the peak position and to the difference of the intensity in the tail. This asymmetry is examined also in paragraph on dispersion surfaces.

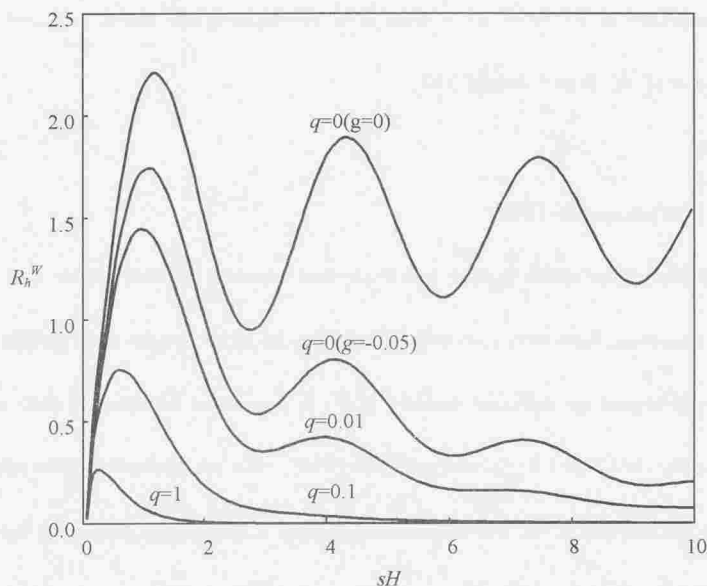


Fig 2.11 The integrated reflecting power in the symmetric Laue case as function of sH .

(v) Integrated reflecting power

Fig 2.11 shows the behavior of the term R_h^w of the integration in (2.87) when $q=0, 0.01, 0.1$ and 1 . A horizontal axis is sH . The pendellösung beat is compared between case of no absorption ($g=0$) and absorption ($g=-0.05$) when $q=0$. When the crystal thickness becomes

infinitely, $R_h^{(w)}$ will converge on $\pi/2$ with no absorption. However, pendellösung beats with absorption rapidly attenuates. $R_h^{(w)}$ of large $|g|$ becomes zero if sH is infinite. The pendellösung beat in the application limit ($q=0.01$) of SIA can be seen until 3 periods. The maximum of $R_h^{(w)}$ in $q=0.1$ is about 0.75, pendellösung beat cannot be seen, and the maximum of $R_h^{(w)}$ in $q=1$ is about 0.27.

2.3.2 Nontransparent Effect

Nontransparent effects are effects that transmitted intensities become weaker than the mean absorption, remarkably in $0 < q < 1$. When $q=0$, since all the energies of the incident X-rays will become the diffracted intensity at $W=0$, transmitted intensities are zero and $sH = (2n-1)\pi/2$ ($n=1,2,\dots$) (see Fig. 2.8). However, this is not the nontransparent effect. There are two ideas in the nontransparent effect. One is the effect of decreasing X-rays remarkably, and another is the effect that completely shuts out X-rays. This paper is based on the opinion that the latter is the solution. Fig. 2.12(a) shows rocking curves which changed sH with 1.88, 3.49 and 4.70 when $q=0.5$, and (b) shows rocking curves which changed q with 0.0099, 0.876 and 0.99 when $sH=4.38$. Each rocking curve of Fig. 2.12 shows the nontransparent effect. When the nontransparent effect occurs, these rocking curves have suggested the special relationship among sH , q , and W .

In order to analyze the nontransparent effect as Fig. 2.12, the wave field in the crystal

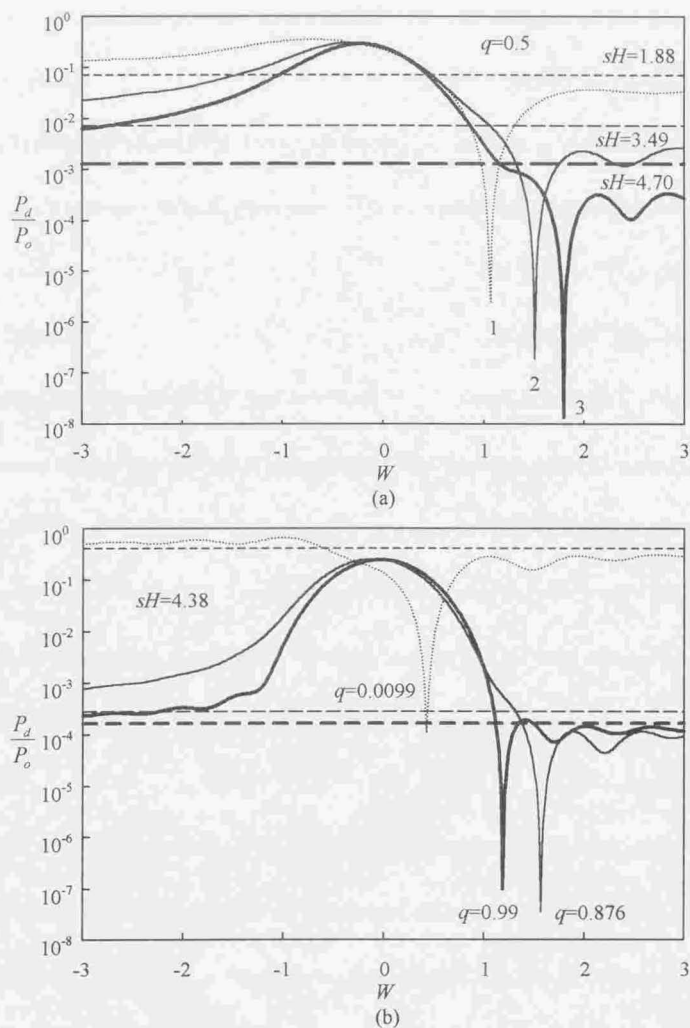


Fig 2.12 The rocking curves of the transmitted wave for $g_0=-1, \delta=0$ when constant q and sH . The three dashed lines represent $\exp(\mu_0 H)$ for the sH , respectively. (a) constant $q=0.5$; $sH=4.70$ (thick solid line), $sH=3.49$ (thin solid line) and $sH=1.88$ (dotted line). (b) constant sH ;

are examined as D_{or} , D_{oi} and D_o . Each two waves connected with transmitted waves are

in the crystal, and the sum of the two waves is shown in the following equation

$$D_o(h) = D_{or}(h) + iD_{oi}(h). \quad (2.99)$$

As shown in the following equation, $D_{or}(h)$ and $D_{oi}(h)$ of (2.99) are the amplitude of the real part and the imaginary part of the wave $D_o(h)$ from every tie point, respectively

$$D_{or}(h) = D_{or}^{(1)}(h) + D_{or}^{(2)}(h), \quad (2.100a)$$

$$D_{oi}(h) = D_{oi}^{(1)}(h) + D_{oi}^{(2)}(h). \quad (2.100b)$$

When $q = 0.5$, $D_o(h)$ (dotted line), $D_{or}(h)$ (solid line) and $D_{oi}(h)$ (dashed line) are shown in Fig 2.13 when $sH = 1.50, 1.88$ and 2.20 . Noticing point A, the intersection point between D_{or} and D_{oi} is positive at $sH = 1.50$. However, the intersection at $sH = 2.20$ is negative. At the midpoint of them, $sH = 1.88$ both just cross where both are 0. The nontransparent effect is understood to occur when the real part and imaginary part of waves in the crystal become zero simultaneously. Therefore, it is quite natural to be called the nontransparent effect as for this phenomenon.

Furthermore, the real part and the imaginary part of $D_o(h)$ will be examined the origin which becomes zero. Fig. 2.14 shows the behaviors of the wave field in the crystal for every tie point when $sH = 1.88$ and $\delta = 0$. Noticing lines (A-A', B-B') in which the nontransparent effect occurs. In A-A', although the amplitude of $D_{or}^{(2)}$ and $D_{or}^{(1)}$ is equal, the sign is opposite. In B-B' similarly, although the amplitude of $D_{oi}^{(1)}$ and $D_{oi}^{(2)}$ is equal, the sign is opposite. That is, nontransparent effect is understood to occur when real parts of the wave of

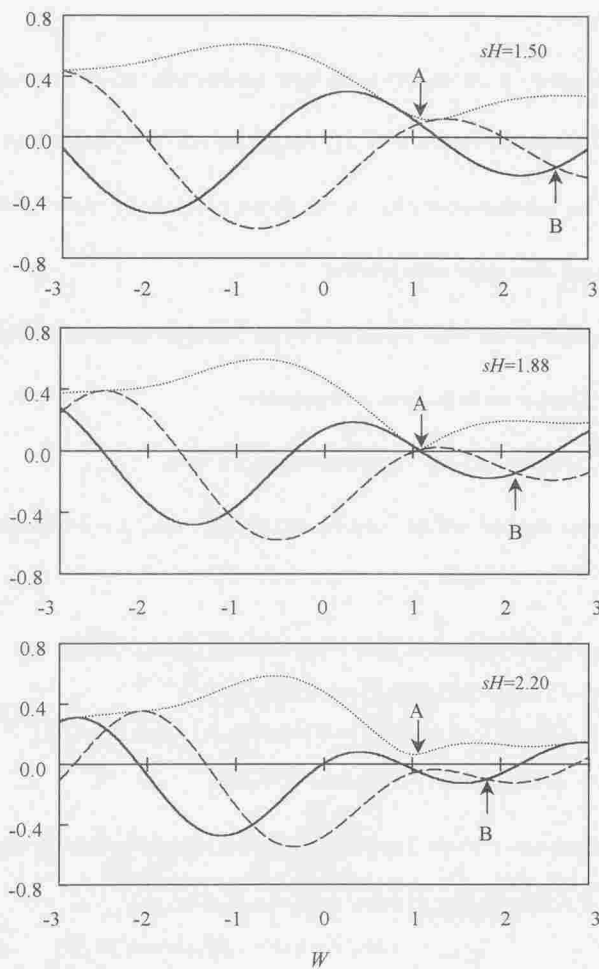


Fig 2.13 The variations of the transmitted wave D_{or} (solid lines), D_{oa} (dashed lines) and $|D_o|$ (dotted lines) for $sH=1.50$ (upper panel), $sH=1.88$ (middle panel), and $sH=2.20$ (lower panel); $q=0.5$, $g_0=-1$ and $\delta=0$.

two tie points negates to each other, and imaginary parts negates under similar

circumstances.

In the case of $\delta = 0$, the reason why the nontransparent effect occurs only by the positive side of W , because the conditions of $|D_{or}^{(2)}| > |D_{or}^{(1)}|$ and $|D_{oi}^{(2)}| > |D_{oi}^{(1)}|$ are always satisfying. However, the nontransparent effect is not always occur in the region of $W > 0$. The nontransparent effect occurs under specified.

The nontransparent effect is generated on the following conditions. The numerator of (2.82 b) is placed as shown in the following equation

$$(W + \sqrt{Q}) \exp(isH\sqrt{Q}) - (W - \sqrt{Q}) \exp(-isH\sqrt{Q}) = x + iy. \quad (2.101)$$

The following equation will be obtained, placing $\sqrt{Q} = \text{Re}\sqrt{Q} + i\text{Im}\sqrt{Q}$ and expands (2.89)

$$\begin{aligned} x + iy = & 2 \left[\text{Im}\sqrt{Q} \sin(sH \text{Re}\sqrt{Q}) - W \cos(sH \text{Re}\sqrt{Q}) \right] \sinh(sH \text{Im}\sqrt{Q}) \\ & + 2 \text{Re}\sqrt{Q} \cos(sH \text{Re}\sqrt{Q}) \cosh(sH \text{Im}\sqrt{Q}) \\ & i \left\{ 2 \left[\text{Im}\sqrt{Q} \cos(sH \text{Re}\sqrt{Q}) + W \sin(sH \text{Re}\sqrt{Q}) \right] \cosh(sH \text{Im}\sqrt{Q}) \right. \\ & \left. - 2 \text{Re}\sqrt{Q} \sin(sH \text{Re}\sqrt{Q}) \sinh(sH \text{Im}\sqrt{Q}) \right\} \end{aligned} \quad (2.102)$$

$|x + iy|^2$ become zero if $x=y=0$. Therefore the following equation is obtained from $x=0$

$$\begin{aligned} & \left[W \cos(sH \text{Re}\sqrt{Q}) - \text{Im}\sqrt{Q} \sin(sH \text{Re}\sqrt{Q}) \right] \sinh(sH \text{Im}\sqrt{Q}) \\ & = \text{Re}\sqrt{Q} \cos(sH \text{Re}\sqrt{Q}) \cosh(sH \text{Im}\sqrt{Q}) \end{aligned} \quad (2.103a)$$

And, the following equation is obtained from $y=0$

$$\begin{aligned} & \left[W \sin(sH \text{Re}\sqrt{Q}) + \text{Im}\sqrt{Q} \cos(sH \text{Re}\sqrt{Q}) \right] \cosh(sH \text{Im}\sqrt{Q}) \\ & = \text{Re}\sqrt{Q} \sin(sH \text{Re}\sqrt{Q}) \sinh(sH \text{Im}\sqrt{Q}) \end{aligned} \quad (2.103b)$$

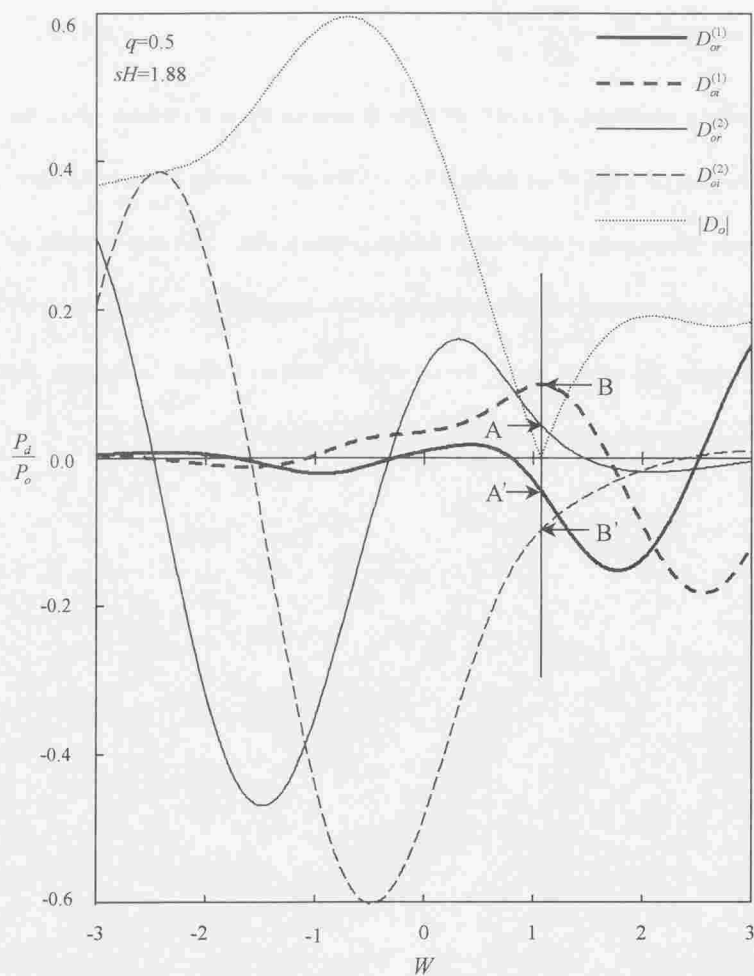


Fig 2.14 The variations of the transmitted wave $D_{or}^{(1)}$ (thick solid line), $D_{or}^{(1)}$ (thick dashed line), $D_{or}^{(2)}$ (thin solid line), $D_{or}^{(2)}$ (thin dashed line) and $|D_o|$ (dotted line) for $sH=1.88$, $q=0.5$, $g_0=-1$ and $\delta=0$.

Following relationship is obtained from (2.103)

$$\tan(2sH \operatorname{Re} \sqrt{Q}) = \frac{2W \operatorname{Im} \sqrt{Q}}{|\sqrt{Q}|^2 - W^2} \quad (2.104)$$

From the relationship of (2.104), in order to generate the nontransparent effect, the conditions of sH , q and W are shown in Fig 2.15. The curved number shown in the figure expresses the sequence in which occurs the nontransparent effect under each condition. In figure(a), the nontransparent effect from 2nd to the 4th shows the tendency that sH becomes the minimum for $q=0.5$, except the primary nontransparent effect. In figure(b), the nontransparent effect shows the tendency that W becomes the maximum for $q=0.5$.

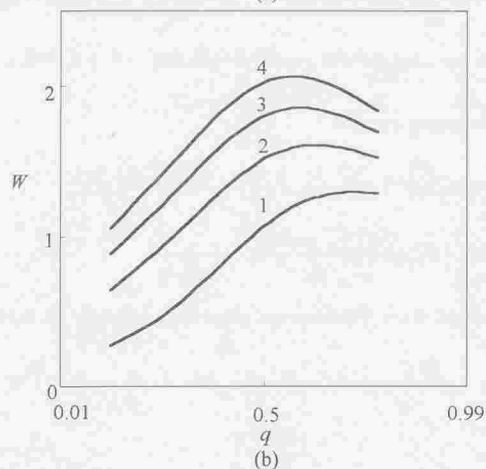
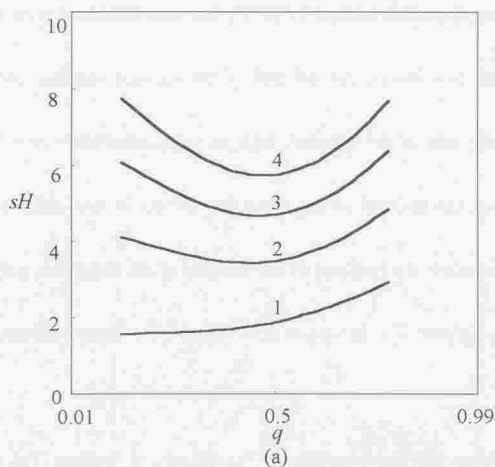


Fig. 2.15 The conditions in which the nontransparent effect occurs.

(a) The relation between q and sH . (b) The relation between q and W .

2.3.3 Dispersion Surface in Laue Case

(i) Introductory

The solution of the dispersion surface by (2.47) has been exist real parts and imaginary parts. In conventional SIA theory, the real part of the solution only has been adopted by neglects the imaginary part of the solution, such as total reflection region in Bragg case when $q=0$. However, the solution of the dispersion surface in this study has the natural complex number. Therefore, the real part of the solution of the dispersion surface is treated equally to the imaginary part. The viewpoint differs from the conventional dynamical theory greatly.

In order to consider the characteristic of the dispersion surface, the conditions of symmetric Laue case are used for this paper ($\beta=\pi/2$ and $-\theta_1 = \theta_2 = \theta_B$). Consequently, (2.47) becomes the following equation

$$(Y' \cos \theta_B)^2 - (X \sin \theta_B)^2 - (Z' \cos \theta_B - \kappa_{oi})^2 = \frac{\kappa_{or}^2 \overline{\chi_h}^2 (1-2q)}{4}, \quad (2.105a)$$

$$Y' \cos \theta_B (Z' \cos \theta_B - \kappa_{oi}) = \frac{\kappa_{or}^2 \overline{\chi_h}^2 p \cos \delta}{4}. \quad (2.105b)$$

The variation of the shape of the dispersion surface is examined for $q=0, 0.5$ and 1 .

(ii) In case of $q=1$

The dispersion surface not considered conventionally in $q=1$. In this case, p on the right-hand side of (2.105 b) is zero. Therefore, there are two cases of $Y' \cos \theta_B = 0$ or $Z' \cos \theta_B - \kappa_{oi} = 0$. The following equation is obtained from $Z' \cos \theta_B - \kappa_{oi} = 0$

$$(X \sin \theta_B)^2 - (Y' \cos \theta_B)^2 = \frac{\kappa_{or}^2 |\chi_h|^2}{4}. \quad (2.106a)$$

The following equation is obtained from $Y' \cos \theta_B = 0$ [6]

$$(X \sin \theta_B)^2 + (Z' \cos \theta_B - \kappa_{oi})^2 = \frac{\kappa_{oi}^2 |\chi_m|^2}{4} \quad (2.106b)$$

The dispersion surface obtained by (2.106) is shown in Fig 2.16. In this figure, the dispersion surface is shown on the 3-dimensional orthogonal coordinates with three axes (X , Y , Z). Axis X is parallel to the crystal surface, Y and Z axes cross orthogonal to X -axis and perpendicularly intersecting each other.

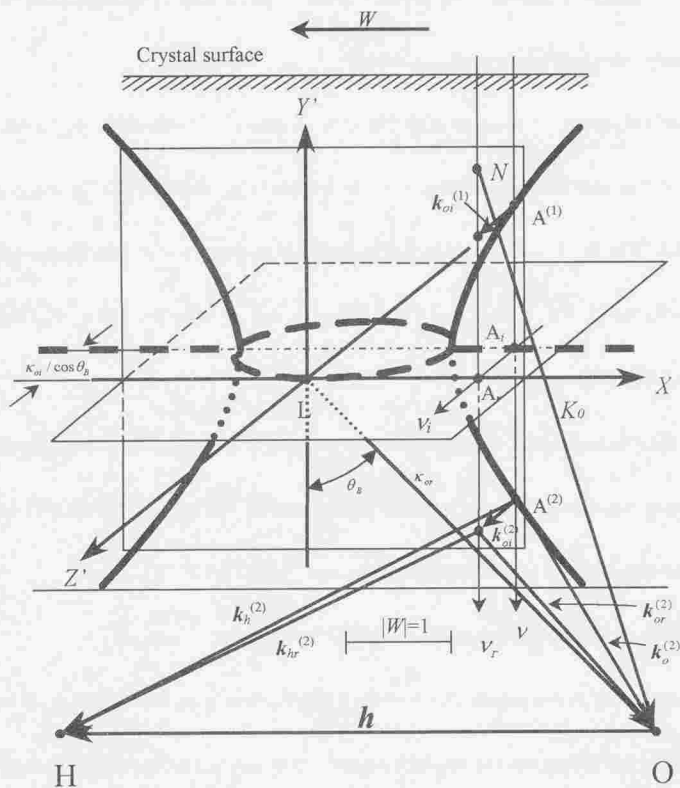
The real part of the solution of (2.106 a) is on plane X - Y shifted by $\kappa_{oi} / \cos \theta_B$ from Z -axis. The real part of the solution is the hyperbola in $|X| \geq |X(|W|=1)|$ and is zero in $|X| < |X(|W|=1)|$. The imaginary part of (2.106 b) is on plane X - Z' and the imaginary part of the solution is the ellipse in $|X| < |X(|W|=1)|$ and is constant value $\kappa_{oi} / \cos \theta_B$ in $|X| \geq |X(|W|=1)|$.

In order to understand the tie point on the complex dispersion surface, let us consider the following two cases. One case is where the normal-line ν is located $|X| \geq |X(|W|=1)|$, and another case is where the normal-line ν is located $|X| < |X(|W|=1)|$.

a) *When normal-line ν is located in $|X| \geq |X(|W|=1)|$*

The tie point in this case is shown in Fig 2.16(a). There is an intersection A_r of between the X -axis and the normal line ν_r which are decided by incident X-rays K_0 . An A_i is the point which carried out $\kappa_{oi} / \cos \theta_B$ movement on Z' -axis, through the A_r . The straight line ν is parallel to ν_r through the A_i , two tie points are $A^{(1)}$ and $A^{(2)}$ which intersections are

waves exist in the crystal, $k_o^{(1)}$ and $k_h^{(1)}$ from $A^{(1)}$, $k_o^{(2)}$ and $k_h^{(2)}$ from $A^{(2)}$.


$$(a) |X| \geq |X(|W|=1)|$$

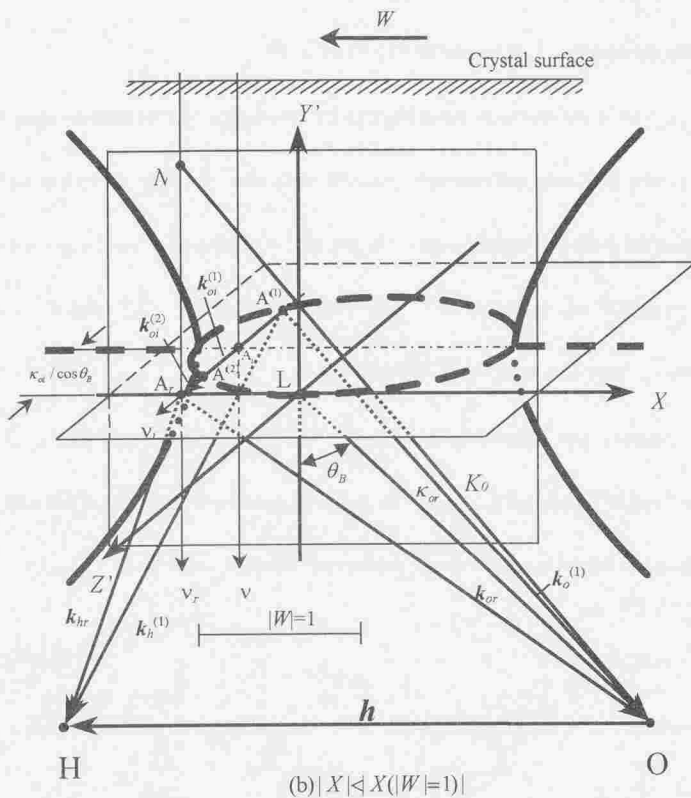


Fig.2.16. The complex dispersion surface in the symmetric Laue case when $q=1$ and $\delta=0$. Thick solid lines are the real parts, thick dashed lines are the imaginary parts.

Since the imaginary part of the dispersion surface is constant value $Z'=\kappa_{oi}/\cos\theta_B$,

$k_{oi}^{(1)}=k_{oi}^{(2)}$. For this reason, no difference of the absorption in waves is caused by tie-point (1)

and (2). There are always two tie points on the real part of dispersion surface whose values

slightly differ. Therefore, the pendellösung beat appears.

b) When normal-line ν is located in $|X| < |X(W=1)|$

The tie point in this case is shown in Fig 2.16(b). The straight line ν_i is on the plane $X-Z$, and is parallel to Z -axis, and intersects perpendicularly with ν_r . Since the real part of the solution of the dispersion surface is zero, the intersection of between ν_i and ellipse which is on an plane $X-Z$ are tie points $A^{(1)}$, $A^{(2)}$. Therefore, since $k_{hr}^{(1)} = k_{hr}^{(2)}$ and $k_{or}^{(1)} = k_{or}^{(2)}$, pendellösung beats does not exist in $|X| < |X(W=1)|$.

The imaginary part of the dispersion surface is ellipse on an plane $X-Z$. $k_{oz}^{(1)}$ is the distance from $A^{(1)}$ to A_r and $k_{oz}^{(2)}$ is $A^{(2)}$ to A_r . Let us consider the meaning of this solution.

These have the following relationship in symmetrical reflective conditions

$$\begin{aligned} k_{oz}^{(j)} &= k_{ozr}^{(j)} + ik_{ozi}^{(j)} \\ &= \kappa_{or} \cos \theta_B + Y^{(j)}. \end{aligned} \quad (2.107)$$

In this equation, j is tie-point number. The following equation is obtained from (2.61)

$$k_{ozi}^{(j)} = \begin{cases} \frac{s}{2\pi} g, & |W| \geq 1 \\ \frac{s}{2\pi} \left[g + (-1)^j \sqrt{1 - W^2} \right], & (|W| < 1) \end{cases} \quad (2.108)$$

g of (2.108) is proportional to the absorption coefficient μ_0 , as shown in (2.98). Therefore,

the absorption is large when $k_{ozi}^{(j)}$ is large. The average length from two tie points to X -axis

is shown in the following equation

$$\frac{k_{ozi}^{(1)} + k_{ozi}^{(2)}}{2} = \frac{s}{2\pi} g = \frac{\kappa_{oi}}{\cos \theta_B}$$

$$= -\frac{\mu_0}{4\pi \cos \theta_B} \quad (2.109)$$

This equation (2.109) means that an average with $k_{oz}^{(1)}$ and $k_{oz}^{(2)}$ is proportional to a mean absorption.

Following, let us consider anomalous transmission in $|X| < |X(W=1)|$. $|k_{oz}^{(2)}| < |k_{oz}^{(1)}|$ is indicated from Fig. 2.16(b). This indicates that the wave with tie-point $A^{(1)}$ is absorbed more greatly than the wave with tie-point $A^{(2)}$. Since the wave with tie-point $A^{(1)}$ is absorbed more greatly than the mean absorption, the wave indicates the anomalous absorption. Conversely since the absorption of the wave with tie-point $A^{(2)}$ is smaller than the mean absorption, the wave indicates the anomalous transmission. In this case in $X=0$ ($W=0$), Z' is zero. Therefore, there will be completely no absorption at all. On the other hand, the wave will tie-point $A^{(1)}$ receives the absorption of the twice of the mean absorption in $X=0$ [7].

As mentioned above, the display of the complex dispersion surface as Fig 2.16 is very convenient to understand the dynamical diffraction by the resonance scattering. However, the description of the figure is not easy. Therefore, the method to share Y -axis and Z' -axis and to use simple drawing planes can be considered. One of drawing is shown in Fig 2.17(a). The complex dispersion surface shown in Fig 2.16 can be analogized from this figure relatively easily. Therefore, we use the shape of Fig 2.17 for the display of the complex dispersion surface henceforth.

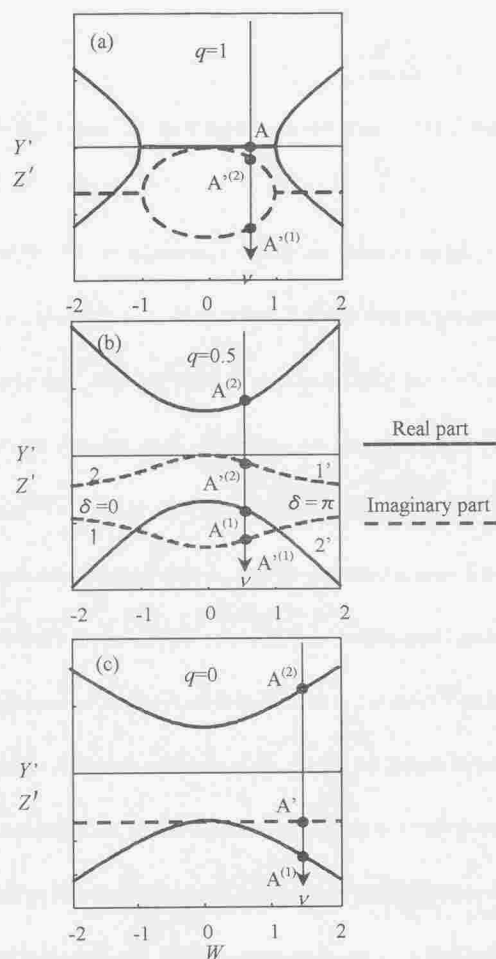


Fig. 2.17. The dispersion surface in the symmetric Laue case. The solid and the dashed curves are the real and the imaginary part of the curves.

$\delta=0$. (a) $q=1.0$, $g_0=-1.0$. (b) $q=0.5$, $g_0=-1.0$. (c) $q=0.0$, $g=-0.1$.

(iii) In case of $q=0$

Let us consider the complex dispersion surface with absorption for $q=0$. If $Y' \cos \theta_B$ is not zero in (2.105), the relationship of the following equation satisfies

$$(Y' \cos \theta_B)^2 - (X \sin \theta_B)^2 = \frac{\kappa_{or}^2 |\chi_{tr}|^2}{4}, \quad (2.110a)$$

$$Z' \cos \theta_B - \kappa_{oi} = 0. \quad (2.110b)$$

The complex dispersion surface of (2.110) is shown in Fig2.17(c). It will guess from the case of $q=1$. The real part of solution (the hyperbola, thick solid line) of this dispersion surface is on the plane X - Y' shifted by $\kappa_{oi} / \cos \theta_B$, Z' axis from the origin L . The imaginary part of the solution is the straight line (thick dashed line) of the constant value which shifted by $\kappa_{oi} / \cos \theta_B$ on an plane X - Z' . The imaginary part of the solution indicates that the wave of tie points 1 and 2 receives the same constant absorption. For this reason, there is neither the anomalous transmission, nor the anomalous absorption. Since the real part of the solution has two value which always differs, the pendellösung beat is observed in the entire regions of $X(W)$.

(iv) In case of $q=0.5$

In Fig 2.17(b) shows the complex dispersion surface when $q=0.5$, $g_0=-1$, $\delta=0$ or $\delta=\pi$. Numbers in the figure expresses the number of the tie point which $\delta=0$ represent as 1 and 2, and $\delta=\pi$ are 1' and 2'. A thick solid line shows the real part of solution, and the thick dashed line shows the imaginary part of the solution. The real part of the solution is similar to change of the solid line of Fig 2.17(c), and the imaginary part of solution is similar to change of the dashed line of Fig 2.17(a). The sections of this dispersion surface are separated

in the entire regions of X (W) in the real and imaginary parts of solutions. In $\delta = 0$, the imaginary part of the solution of the tie point $A^{(2)}$ is zero at $X = 0$ ($W = 0$) and the wave shows anomalous transmission as in (a), does not indicate absorption. The imaginary solution of the tie point $A^{(1)}$ proportional to absorption twice as many as the mean absorption at $X = 0$. Thus, the wave with the tie point $A^{(2)}$ indicates the anomalous transmission and the wave with the tie point $A^{(1)}$ indicates the anomalous absorption when $\delta = 0$.

Let us consider the following asymmetry of the transmitted rocking curve when $q = 0.5$. In the Fig. 2.14, the amplitude of the wave field with tie-point 2 is larger than one with tie-point 1 in the positive side of X ($W < 0$), it is the contrary in the negative side of X . However, the absorption is symmetry with $X = 0$. Therefore, since the amplitude of the wave field in the crystal is asymmetry with $X = 0$, the rocking curve of the transmitted intensity becomes asymmetry.

On the other hand, if $\delta = \pi$, the amplitude of the wave field with the tie point 2 is smaller than one of the tie point 1 in the positive side of X , and the negative side is the contrary. Therefore, in the rocking curve of the transmitted intensity in $\delta = 0$, the asymmetry is opposite that in $\delta = \pi$. Although the real part of the solution of dispersion surfaces of $q = 0$ and $q = 1$ was hyperbola, there are shown that both are conjugations to each other. By using a complex dispersion surface as mentioned above, the absorption can be understand from

diagrams of imaginary part of solutions. The expression of the dispersion surface is natural to the complex number.

2.3.4. Energy Flow

In this section, we consider the energy flow in the crystal with q value using a Poynting vector. According to the conventional dynamical theory, when there is no absorption, or when it is so small that absorption neglected, the Poynting vector is the normal to the real part of the dispersion surface[15]. Assuming the Poynting vector is the normal to the hyperbola in Fig 2.16 when $q=1$, the direction of the Poynting vector at $|W|=1$ is parallel to the crystal surface. However, the X-rays pass through the crystal. If the Poynting vector is the normal to the hyperbola when $q=1$, these X-rays cannot penetrate the crystal. Therefore, the interpretation is not realistic. That is, in $q=1$, it does not satisfy assumption that the Poynting vector is the normal to the real part of the dispersion surface. Therefore, the purpose of this paragraph is examined of the relationship between the Poynting vector and the real part of the dispersion surface as q changes.

(i) The direction of energy flow

In the case of symmetric Laue reflection, because $\beta = \pi/2$, (2.47) of the dispersion surface is modified as following equation

$$Y^2 \cos^2 \theta_B - X^2 \sin^2 \theta_B - 2i\kappa_{0i} Y \cos \theta_B - \kappa_{0i}^2 = \frac{1}{4} \kappa_{or}^2 \overline{\chi_n^2} (1 - 2q + 2ip \cos \delta). \quad (2.112)$$

The following relationship exists among $\theta_B, \beta, \theta_1$ and θ_2 in Fig.2.2

$$\theta_B + \beta = -\theta_1 + \frac{\pi}{2}, \quad \theta_B - \beta = -\theta_2 - \frac{\pi}{2}. \quad (2.113)$$

The following relationship is obtained from $\beta = \pi/2$

$$-\sin \theta_1 = \sin \theta_2 = \sin \theta_B, \quad (2.114)$$

$$\cos \theta_1 = \cos \theta_2 = \cos \theta_B. \quad (2.115)$$

Differentiating (2.48) with respect to X and the following equation is obtained, respectively

$$-X \sin^2 \theta_B + \left(Y' \frac{dY'}{dX} - Z' \frac{dZ'}{dX} \right) \cos^2 \theta_B + \kappa_{0i} \cos \theta_B \frac{dZ'}{dX} = 0, \quad (2.116a)$$

$$\left(Y' \frac{dZ'}{dX} + Z' \frac{dY'}{dX} \right) \cos^2 \theta_B - \kappa_{0i} \cos \theta_B \frac{dY'}{dX} = 0. \quad (2.116b)$$

Calculating $\frac{dZ'}{dX}$ from (2.116b) and substituting it in (2.116a) and the following equation is

obtained

$$\frac{dY'}{dX} = \frac{XY' \sin^2 \theta_B}{Y'^2 \cos^2 \theta_B + (\kappa_{0i} - Z' \cos \theta_B)^2}. \quad (2.117)$$

As shown in Fig 2.18, assuming σ is an angle which shaped by the tangent in the point (X, Y')

of the real part of the dispersion surface and axis X , $\tan \sigma$ is as follows

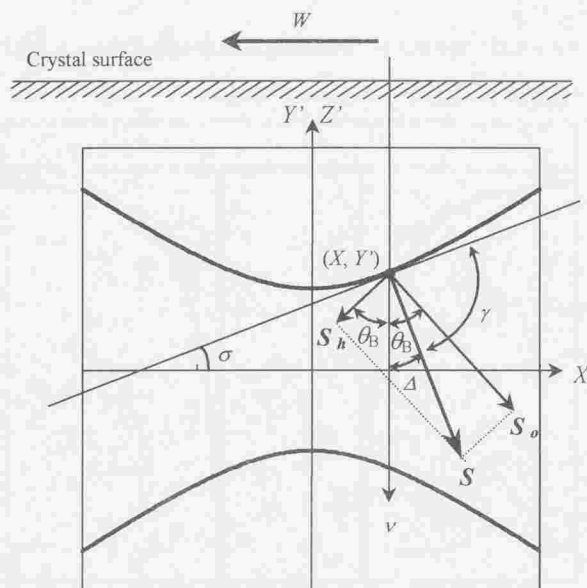


Fig 2.18 Geometrical construction of Poynting's vector S and the dispersion surface.

$$\tan \sigma = \frac{dY'}{dX}. \quad (2.118)$$

Let us Δ is an angle that shaped by Poynting vector and diffracting lattice surface, the following equation will be established from Fig.2.18

$$\tan \Delta = \frac{|R^{(j)}|^2 - 1}{|R^{(j)}|^2 + 1} \tan \theta_B. \quad (2.119)$$

Where, j is the number of the tie point. Consequently, the angler between the Poynting vector and the real part of the dispersion surface is given by the following equation [14]

$$\tan \gamma = \cot(|\sigma + \Delta|). \quad (2.120)$$

If changes $q = 0.0, 0.1, 0.5, 0.9$ and 1.0 , calculating from (2.120) is shown in Fig. 2.19.

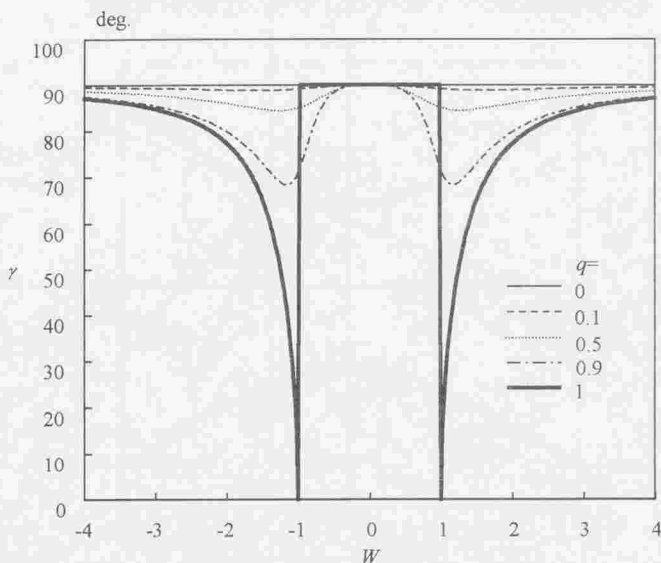


Fig.2.19 The variation of γ with respect to W for different values of q in the symmetric Laue case.

a) In case of $q=0$

When there is no absorption, Kato[15] has proven that Poynting vectors are the normal to the dispersion surface. However according to this study, Poynting vectors are always the normal to the dispersion surface if $q = 0$, regardless of whether or not absorption functions. This result is in agreement with the results of Kato(1958)[15], Ewald(1958)[16], and Battermann&Cole(1964)[5]. However, the above treatment is not neglecting absorption. In

$q=0\sim 0.1$, γ is within the limits of 90° to 89.4° . Therefore, in $q<0.1$, Poynting vectors are almost the normal to the real part of the dispersion surface.

b) *In case of $0.5<q<1$*

In $q=0.5$ and $W\gg 1$, Poynting vectors are the normal to the real part of the dispersion surface. However, when W approaches -1 gradually, γ deviate from 90° gradually, and γ has the minimum value of 84.5° at $W=-1.26$, and γ becomes large increasing W and will become 90° at $W=0$. Thus, if q becomes about 0.5 , it cannot say that Poynting vectors are the normal to the dispersion surface. If $q=0.9$, γ will become 68.3° at $|W|=1.16$.

c) *In case of $q=1$*

In this case, γ shows a very big change, as shown in Fig.2.19. If $|W|\gg 1$, as in case of other q , $\gamma=90^\circ$. However, γ gradually deviates from 90° when $|W|$ approaches $|1|$, becoming $\gamma=0$ at $|W|=1$. That is, the Poynting vector and the real part of the dispersion surface are parallel at $|W|=1$. This result shows physical meaning which the energy in the crystal flow along with diffracting lattice plane, and since X-rays penetrate the crystal, this conclusion does not have inconsistency. As shown in Fig.2.16, the real part of solution the dispersion surface is zero in $|W|<1$ when $q=1$. On the other hand, γ is 90 degrees in $|W|<1$ as Fig.2.19. That is, if $|W|<1$, the Poynting vector is perpendicular to the real part of the dispersion surface and energy flows along with the diffracting lattice plane. This result not inconsistency physically also.

The above result in $q=0$, even when there is absorption, it is shown that Poynting vectors are the normal to the real part of the dispersion surface. Moreover, in $W=0$, Poynting vectors are the normal to the real part of the dispersion surface, regardless of q value. However, excepting the above-mentioned case, Poynting vectors are not the normal to the real part of the dispersion surface near $W=1$. The tendency becomes so remarkable that q approaches 1.

(ii) Quantitative treatment of the energy flow

This section is examined the quantity of the Poynting vector by change of q and W . In (2.88), if direction z is an inward direction of the crystal, z is in agreement with crystal thickness H on the under surface of the crystal. Therefore, magnitude $S^{(j)}$ of Poynting vector \vec{S} for every tie point is as follows in the deepness z of the crystal

$$S^{(j)} = \frac{c}{8\pi} \exp(4\pi k_{oz} z) \left[|D_o^{(j)}|^2 + |D_h^{(j)}|^2 \right]. \quad (2.121)$$

The term \exp in (2.121) is an attenuation from by the absorption. [] is in the second term shows that the diffracted and the transmitted waves are united and propagating in of the crystal. Expression of this equation is the same as that of the conventional equation. However, the contents in the absorption term differ as for SIA. The following equation modifies the \exp term of (2.121) and is obtained

$$\exp(4\pi k_{oz} z) = \exp \left\{ 2sz \left[g + (-1)^j \operatorname{Im} \sqrt{Q} \right] \right\}. \quad (2.122)$$

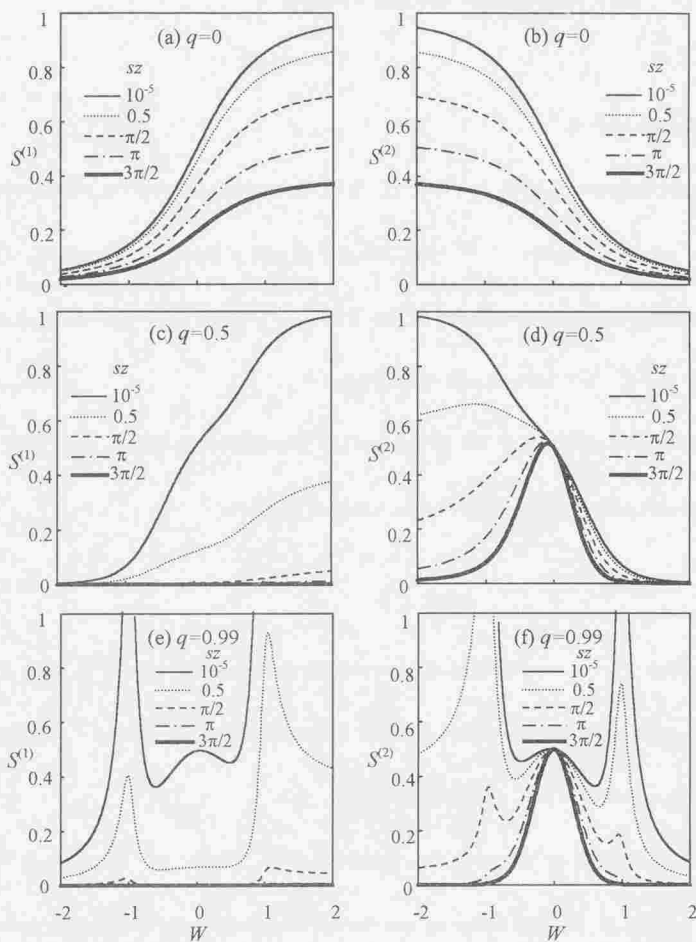


Fig 2.20 The variation of the amplitude of the Poynting vector when $\delta=0$.
 (a) $q=0$ for $S^{(1)}$, (b) $q=0$ for $S^{(2)}$, (c) $q=0.5$ for $S^{(1)}$, (d) $q=0.5$ for $S^{(2)}$,
 (e) $q=0.99$ for $S^{(1)}$, (f) $q=0.99$ for $S^{(2)}$.

Fig.2.20 shows $S^{(j)} = 0, 0.5, 0.99$ when sz is changed to $10^{-5}, 0.5, \pi/2, \pi$, and $3\pi/2$ when q

is 0, 0.5, and 0.99. In this case, $c/8\pi$ was neglected.

a) *In case of $q=0$*

As examined in 2.3.1-ii, $g=-0.1$ ($\chi_{0f} \neq 0$) was set taking absorption into consideration. The calculation results of $S^{(1)}$ and $S^{(2)}$ are shown in Figs.2.20 (a) and (b). $S^{(1)}$ will increase gradually with increasing W , conversely, $S^{(2)}$ will decrease with increasing W . And, $S^{(1)}$ and $S^{(2)}$ will decrease with increasing z .

Reduction of $S^{(1)}$ and $S^{(2)}$ by increase of z is interpreted as follows. If $q=0$, $\text{Im}\sqrt{Q}=0$ will result, and (2.122) is shown by the following equation

$$\exp(4\pi k_{oz}^{(j)} z) = \exp\left(-\frac{\mu_0 z}{\cos\theta_B}\right). \quad (2.123)$$

However, $k_{oz} = K_o$ was assumed. If z increases in the attenuation term of (2.123), $S^{(1)}$ and $S^{(2)}$ will become small exponentially. Thus, z dependability of $S^{(1)}$ and $S^{(2)}$ is understood.

b) *In case of $q=0.5$*

Changing sz to 10^{-5} to $3\pi/2$, calculation results of $S^{(1)}$ and $S^{(2)}$ are shown in Fig.2.20 (c) and (d). In this case, excepting near the surface ($sz=10^{-5}$), the difference in tie points 1 and 2 appears in $S^{(j)}$. As shown in (c), $S^{(1)}$ increases gradually increasing W . However, if z increases, $S^{(1)}$ will become small remarkably unlike (a). And, when z increases as $3\pi/2$, $S^{(1)}$ is almost zero.

On the other hand, if sz becomes above $\pi/2$, as for $S^{(2)}$ of (d), the peak will be shaped near $W=0$. If sz increases, although the peak will become sharp gradually, the peak height converges on constant value (0.5). Since the exp term of (2.122) is set to 1, $S^{(2)}$ is not dependent on z and becomes constant value. The reason is that $k_{oz}^{(2)}$ by the tie point 2 on the imaginary part of the dispersion surface located in zero at $W=0$.

c) In case of $q=0.99$

In $q=1$, since the denominator \sqrt{Q} is set to $\sqrt{W^2-1}$ from (2.73), D_o diverge at $|W|=1$. For this reason, $S^{(j)}$ is not calculated at $|W|=1$ (the problem of this divergence is examined the standing wave in the crystal). Then, this paragraph is examined $S^{(j)}$ for $q=0.99$.

$S^{(1)}$ and $S^{(2)}$ by change of sz are shown in Fig.2.20(e),(f). In $|W|=1$, there are peaks of $S^{(1)}$ and $S^{(2)}$, for $sz < \pi/2$. $S^{(1)}$ and $S^{(2)}$ have the peak at near the crystal surface ($sz=10^{-5}$) at $W=0$. However, the peak of $S^{(1)}$ at $W=0$ will disappear with increasing sz , and the valley is shaped, and $S^{(1)}$ is almost zero when $sz=3\pi/2$. $S^{(2)}$ shows the peak like $S^{(1)}$ at $W=0$ in near the crystal surface ($sz=10^{-5}$). The peak of $S^{(2)}$ at $W=0$ will become sharp with increasing sz unlike $S^{(1)}$, and the peak height converges on constant value (0.5).

Poynting vectors $S^{(1)}$ and $S^{(2)}$ decrease by the mean absorption with increasing sz when $q=0$. However, in case of $q \neq 0$, the change of $S^{(1)}$ and $S^{(2)}$ are difference with increasing sz . If sz increases, $S^{(1)}$ will decrease remarkably by the anomalous absorption. $S^{(2)}$ will converge on constant value (0.5) by the anomalous transmission at $W=0$.